Gondwana Research 109 (2022) 183–204

Contents lists available at ScienceDirect

Gondwana Research

journal homepage: www.elsevier.com/locate/gr

Provenance and depositional setting of the Buem structural unit (Ghana): Implications for the paleogeographic reconstruction of the West African and Amazonian cratons in Rodinia

Daniel Kwayisi [a,b,*], Jeremie Lehmann [b], Marlina Elburg [b]

[a] Department of Earth Science, University of Ghana, Main Campus, Legon, Ghana
[b] Department of Geology, University of Johannesburg, Auckland Park Kingsway Campus, Johannesburg, South Africa

ARTICLE INFO

Article history:
Received 9 August 2021
Revised 11 March 2022
Accepted 28 April 2022
Available online 4 May 2022
Handling Editor: J.G. Meert

Keywords:
Detrital zircon geochronology
Gondwana
Rodinia
West African Craton
Amazonian Craton
Passive margin

ABSTRACT

We present new field, petrological and geochemical data, combined with U-Pb zircon ages and Lu-Hf isotope compositions for the sandstones of the Neoproterozoic Buem structural unit (BSU) of the Dahomeyide belt, and whole-rock geochemical data of BSU shale to investigate their provenance and depositional setting. The BSU contains siliciclastic sequences and fragments of oceanic lithosphere (pillow lavas, gabbro, and peridotite) that have archived the entire evolution of the Ediacaran West Gondwana Orogen (WGO), from early accretion to final amalgamation of the West African Craton (WAC) with the Benino-Nigerian Shield. Three broad groups of samples exist within the BSU in Ghana: those with dominantly older age fractions of 2300 – 1800 Ma, represented by samples from the base of the BSU; those with prominent 1700 – 1100 Ma zircons, occupying the middle part of the BSU; and those with significant 1000 – 970 Ma age fractions, forming the uppermost part of the BSU. Results from this study, together with published data on the BSU, and adjacent Togo structural unit and Voltaian Supergroup, reveal two main sedimentary sequences in the Dahomeyide belt, i.e., passive margin and foreland basin sequences with three potential provenances: Amazonian Craton, Benino-Nigerian Shield, ± WAC. This interpretation resembles that for the sedimentary rocks of the Borborema Province, NE Brazil, which implies similar evolution along the WGO. Thus, a long, >2500 km passive margin basin developed at 1000 – 700 Ma, which was subsequently inverted during the Braziliano/Pan-African plate convergence and collision, and the concomitant formation of the foreland basin during the assembly of the supercontinent Gondwana. Because a greater portion of the detritus in the BSU is probably from the Amazonian Craton, we propose that the WAC and the Amazonian Craton adjoined each other from the Paleoproterozoic onward within the supercontinents Rodinia and Gondwana, until the opening of the Atlantic Ocean.

1. Introduction

The Ediacaran West Gondwana Orogen (WGO) resulted in the amalgamation of four cratonic nuclei, i.e., the West African and Amazonian cratons to the west, and São Francisco Craton, and Sahara Metacraton to the east, during the Brasiliano/Pan-African orogeny (Fig. 1 inset; Caby, 2003; Cordani et al., 2013; Ganade de Araujo et al., 2014a). The WGO developed from West Africa to Central Brazil over >4000 km and records a long-lived (780 to 640 Ma, U-Pb ages of arc-related granitoids) subduction system since the early Neoproterozoic (Caby, 2003; Cordani et al., 2013; Ganade de Araujo et al., 2014a, 2016). The WGO accretionary orogenic evolution was terminated at ~ 620 – 610 Ma when several newly formed sections of oceanic crust, intra-oceanic and continental arcs were caught up in the collision between the Amazonian and West African cratons on the one side, against the São Francisco Craton and Saharan Metacraton on the other during the Brasiliano/Pan-African orogeny (Caby, 2003; Cordani et al., 2013; Ganade de Araujo et al., 2014a, Guillot et al., 2019). Four segments (Dahomeyide, Pharusian and Brazilia belts and Borborema Province) form the WGO (Fig. 1; Ganade de Araujo et al., 2016). The Buem structural unit (BSU) of the Dahomeyide belt is a key crustal component for unravelling the evolution of the WGO system from early passive margin formation to final amalgamation (Fig. 1a). This is because the BSU is situated in the lower plate, and contains siliciclastic sequences and fragments of oceanic lithosphere (Fig. 2 and Fig. 3) that archive the entire evolution of the WGO, from early

* Corresponding author.
E-mail address: dkwayisi@ug.edu.gh (D. Kwayisi).

https://doi.org/10.1016/j.gr.2022.04.020
1342-937X/

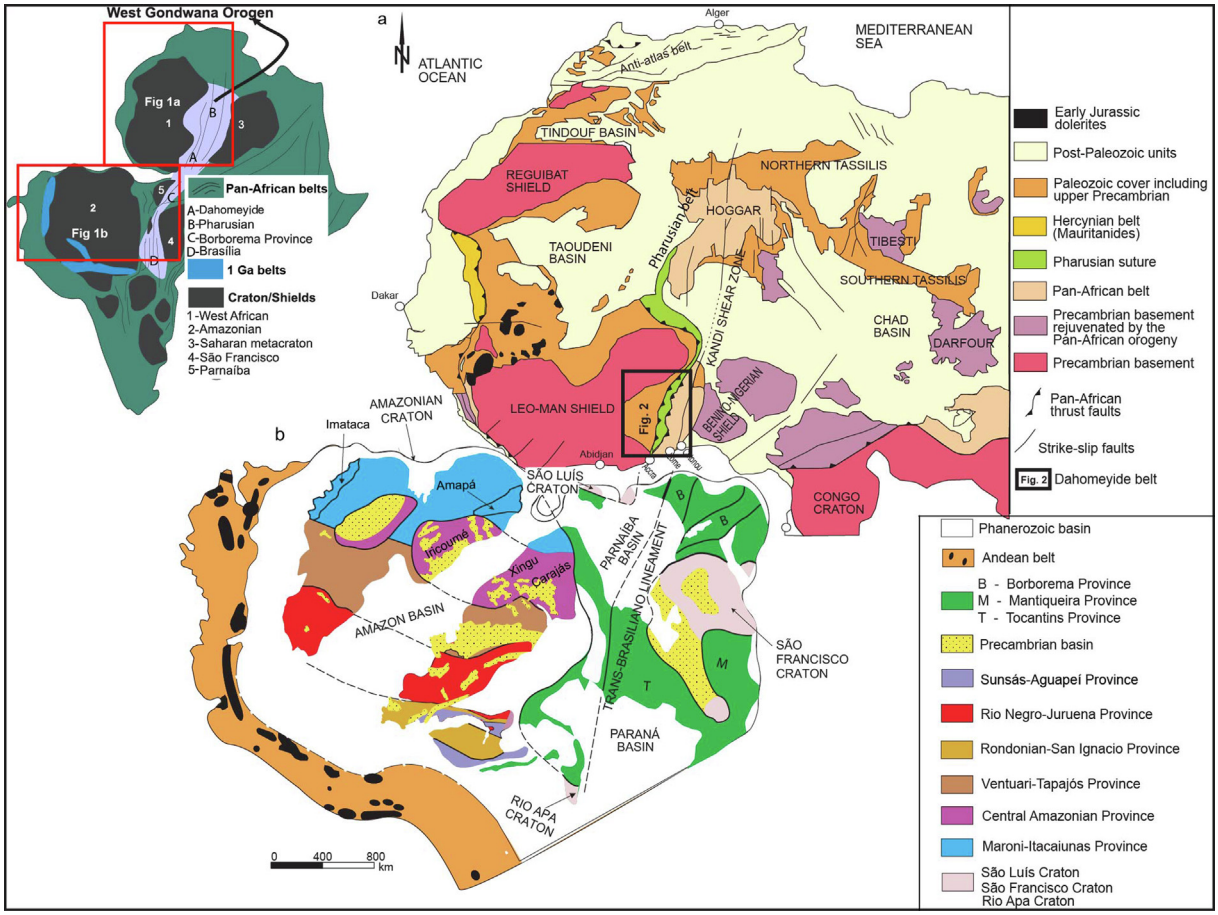

Fig. 1. (a) Geological map of West Africa (after Guillot et al., 2019) and (b) Geological map of South America (after Cordani and Teixeira, 2007) arranged in Gondwana position (before the opening of the Atlantic Ocean; Gray et al., 2008). The inset is the map of West Gondwana Orogen (). adapted from Ganade de Araujo et al., 2016

accretion to final amalgamation of the West African Craton (WAC) with the Benino-Nigerian Shield (i.e., the leading western edge of the Saharan Metacraton; Fig. 1a; e.g. Affaton et al., 1991; Attoh, 1998; Trompette, 2000).

Based on petrographic and geochemical studies of the sandstones from the BSU (upper and lower parts of the stratigraphy), Osae et al. (2006) proposed that the sandstones were deposited in a passive margin setting and received detritus probably from the WAC. In contrast, Kalsbeek et al. (2008) suggested that a significant amount of the detritus for the sandstones of the BSU was sourced from the Amazonian Craton, based on the abundance of U-Pb detrital zircon age fractions between 1700 and 1000 Ma from the upper and lower parts of the BSU, which are absent on the WAC, but common in the Amazonian Craton. Ganade de Araujo et al. (2016) inferred that the uppermost part of the BSU formed as foreland deposits with detritus originating from the BNS based on the significant proportion of detrital zircon U-Pb ages of 900 – 600 Ma, an age group that is absent as a proto-source on the WAC. These studies suggest that the tectonostratigraphic evolution of the BSU possibly records temporal variations in the provenance of the sediments (WAC, Amazonian Craton, Benini-Nigerian Shield), and competition between different sources at the same time (WAC vs Amazonian Craton). They also highlight the need for a detailed geochemical and provenance investigation of the entire BSU stratigraphy for constraining (i) the crustal evolution of the proto-source(s), (ii) the possible connection with the Amazonian Craton, (iii) timing of tectonic inversion from rifting to convergence, and (iv) the overall geodynamic evolution of the external zone of the Dahomeyide belt.

To this end, this study presents, in addition to detrital U-Pb ages for the entire BSU, the first Lu-Hf isotope zircon compositions of the sandstone, and whole-rock geochemical data of shale from the BSU. The results of this study show that the BSU sedimentary rocks were deposited in a passive margin basin, with detritus accumulated from both the WAC and Amazonian Craton, with a greater proportion from the latter. The results provide constraints for the discussion on the assembly of West Gondwana during the Brasiliano/Pan-African orogeny and reconstruction of the pre-Gondwana position of the WAC with respect to the Amazonian Craton in the supercontinent Rodinia.

2. Geological setting

2.1. Regional Geological background

The West African Craton (WAC) is composed of granitoids and greenstone belts with associated sedimentary basins (Fig. 1a; Abouchami et al., 1990; Kouamelan et al., 1997; Baratoux et al., 2011). The WAC formed during three main tectonomagmatic and metamorphic events at ~ 3200 – 3000 Ma (Leonian events), 2900 – 2700 Ma (Liberian events), and ~ 2250 – 2060 Ma (Eburnean orogeny, e.g. Baratoux et al., 2011; Tshibubudze et al., 2013; Sakyi et al., 2014; Anum et al., 2015; Kouamelan et al., 2015; Block et al., 2016). The WAC was stabilized during the Eburnean orogeny and was not affected by any other major orogenic events until its incorporation into West Gondwana during the Neoproterozoic Pan-African orogeny (Villeneuve and Cornée, 1994; Deynoux

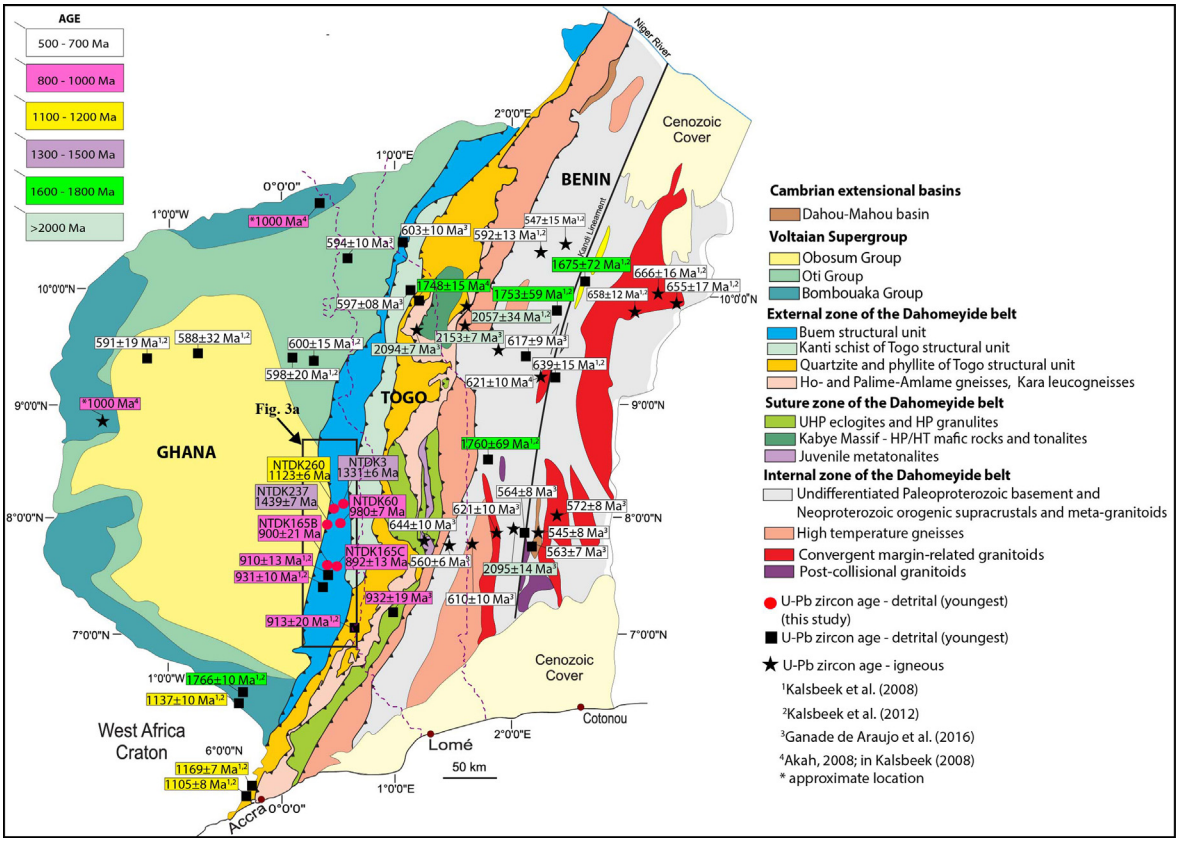

Fig. 2. Geological map of Ghana, Togo and Benin illustrating the context of the Volta Basin, and the Dahomeyide belt (modified after Ganade de Araujo et al., 2016).

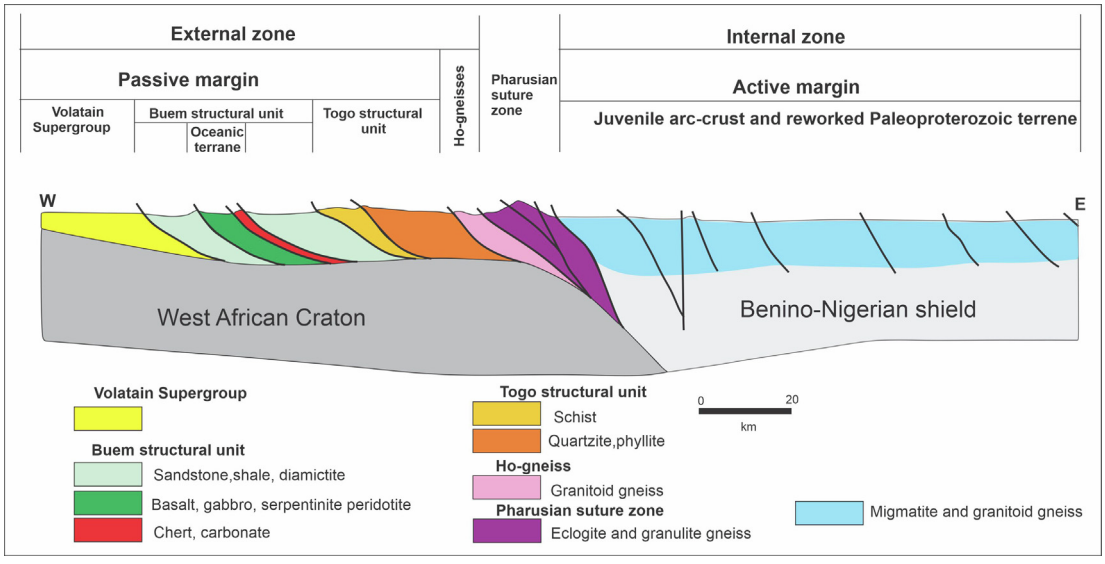

Fig. 3. West-east cross-section of the Dahomeyide belt showing the relationship between the Buem and Togo structural units, and Voltaian Supergroup (modified after Guillot et al., 2019).

et al., 2006; Ennih and Liégeois, 2008). The WAC is covered by the late Meso- and Neoproterozoic sedimentary rocks of the Taoudeni basin (Rooney et al., 2010; Kah et al., 2012) and transected by several generations of dolerite dyke swarms and associated sills with ages ranging from ~ 1700 to 200 Ma (Jessel et al., 2015; Baratoux et al., 2019).

The Amazonian Craton (Fig. 1b) consist of four main Archean blocks (Imataca, Amapá, Carajás, and Xingu-Iricoumé blocks) dated at 3300 – 2600 Ma, which were stabilized around 2100 Ma during the Transamazonian orogeny (2180 – 1950 Ma) (Ledru et al., 1994; Tassinari et al., 2001; Lofan et al., 2003; Cordani et al., 2009; Neto and Lofan, 2019). The Transamazonian orogeny resulted in the formation of greenstones and TTGs (2190 – 2130 Ma), high-grade metamorphic (2070 – 2030 Ma) and felsic volcanic (2000 – 1800 Ma) belts of the Maroni-Itacaiúnas and Ventuari-Tapajós provinces (Fig. 1b; Delor et al., 2003;

Rosa-Costa et al., 2006; Cordani and Teixeira, 2007). Other Proterozoic orogenic belts found within the Amazonian Craton include the 1780 – 1550 Ma Rio Negro-Juruena, 1500 – 1300 Ma belt Rondonian-San Ignacio, and 1250 – 900 Ma Sunsan-Aguapeí orogenic belts (e.g., Santos, 2003; Tassinari et al., 2004; Boger et al., 2005; Cordani and Teixeira, 2007). The eastern margin of the Amazonian Craton is occupied by the 700 – 500 Ma Brasiliano orogenic belt (Borborema Province), which forms the southern section of the WGO, marking the collision between the Amazonian and São Francisco cratons (Cordani and Teixeira, 2007; Ganade de Araujo et al., 2014a, b).

The WAC and Amazonian Craton have been proposed to be connected from 2.0 Ga until their breakup in the Cretaceous (Rogers, 1996; Trompette, 1994; Rogers and Santosh, 2002). Nonetheless, the connection of the WAC with the Amazonian Craton in the Mesoproterozoic and early Neoproterozoic is poorly constrained (Tohver et al., 2006). From paleomagnetic data, the Amazonian Craton is positioned close to the WAC in almost all the reconstructions of the supercontinent Rodinia (1200 – 1000 Ma) (e.g., Evans, 2009, 2013). An Amazonian-WAC connection during the Mesoproterozoic and early Neoproterozoic is also supported by Baratoux et al. (2019) and Antonio et al. (2021) using U-Pb baddeleyite ages and paleomagnetic data from dolerite dyke swarms respectively. The WAC-Amazonian connection is only supported by paleomagnetic data and correlated dyke swarms. Thus, a detailed sedimentary/stratigraphic study to test this proposed connection is necessary.

The Dahomeyide belt, which forms the central section of the WGO, occupies the southeastern margin of the WAC (Fig. 1a and 2; e.g., Attoh et al., 1997; Attoh and Nude, 2008; Ganade de Araujo et al., 2014a). This belt extends from the southeastern coast of Ghana to Nigeria through Togo and Benin and is about 1000 km long (Affaton et al., 1991; Attoh et al., 1997; Agbossoumondé et al., 2001). The Dahomeyide belt formed as a result of the closure of the Pharusian Ocean during convergence, leading to continent–continent collision between the WAC and Benino-Nigerian Shield (Affaton et al., 1991; Attoh et al., 1997; Agbossoumondé et al., 2001; Cordani et al., 2003; Duclaux et al., 2006). The Dahomeyide belt comprises three main zones. The external zone to the west is in a lower plate position and consists of inverted passive margin sequences of the Buem and Togo structural units, with fragments of oceanic lithosphere in the former (Fig. 2 and Fig. 3; Ghana National Geological Mapping Project, 2009; Kwayisi et al., 2020). The basement of the external zone is interpreted to be underthrust WAC Eburnean crust, based on geophysical and structural interpretations (Kwayisi et al., 2020), and in agreement with Paleoproterozoic gneisses occurring in tectonic windows within the passive margin sequences (the Ho-gneisses e.g., Agyei et al., 1987; Attoh and Nude, 2008; Aidoo et al., 2014). The internal zone to the east is composed of Paleoproterozoic granitoids and gneisses (2190 – 2140 Ma) of the Benino-Nigerian Shield that were intruded by magmatic arc plutons at 670 – 610 Ma and post-collisional plutons at 580 – 540 Ma (Kalsbeek et al., 2012; Attoh et al., 2013; Ganade de Araujo et al., 2016). Arc magmatism may be as old as 780 Ma, which is the age of detrital zircon grains from *syn*-orogenic migmatite (Ganade de Araujo et al., 2016). The external and internal zones are separated by a well-defined suture zone of high-pressure (HP: eclogite and granulite) metamorphic rocks, with protolith ages at ~ 800 Ma, and peak metamorphism at 610 ± 5 Ma (Attoh et al., 1991; Affaton et al., 2000; Berger et al., 2011). Exhumation of the HP rocks at 600 – 570 Ma marks the end of collision (Attoh et al., 1997, 2007).

2.2. Geology of the study area

Correlation between the Buem and Togo structural units and the Voltaian Supergroup is a matter of ongoing debate. Although the contacts between these three units are tectonic (Figs. 2 and 3), there is a general increase in metamorphic conditions from west to east, from unmetamorphosed in the Voltaian Supergroup, prehnite-pumpellyite to greenschist facies in the BSU (Affaton et al., 1997; Nude et al., 2015; Kwayisi et al., 2020) and greenschist to lower amphibolite facies in the Togo structural unit (Adjei and Tetteh, 1997; Attoh et al., 1997). This is somewhat correlated with an eastward increase in deformation intensity, as the generally flat-lying Voltaian Supergroup shows steep dips at its eastern margin (Grant, 1969).

Fig. 4 summarises the various correlations and classification schemes proposed in the literature. Pioneering work considered the Buem and Togo structural units to be older than the Voltaian Supergroup, because of their higher degree of deformation and metamorphism (Fig. 4a; Junner and Hirst, 1946). However, the recognition of the characteristic "Triad" of the Kodjari-Buipe Subgroup of the Oti Group in both the Buem and Togo structural units led Affaton (1990), Kalsbeek et al. (2008), and Anani et al. (2019) to infer that the Buem and the Togo structural units are the lateral deformed and metamorphosed equivalents of the Voltaian Supergroup (Table 1; Fig. 4g). Based on the similarity in detrital zircon age distributions between the Voltaian Supergroup, the Togo and Buem structural units, Kalsbeek et al. (2008) and Ganade de Araujo et al. (2016) proposed that the three units were deposited in similar passive margin and foreland basins (Table 1). The maximum depositional age for the BSU rocks with passive margin characteristics is ~ 950 Ma, and these rocks correlate with the passive margin rocks of the Bombouaka Group of the Voltaian Supergroup and quartzite of the TSU (Kalsbeek et al., 2008; Ganade de Araujo et al., 2016). The maximum depositional age for the uppermost sedimentary rocks of BSU is ~ 600 Ma, suggesting derivation from the BNS, and correlation with the Oti and Obosum groups of the Voltaian Supergroup and the Kanti schist of the TSU (Ganade de Araujo et al., 2016).

The 5 – 7 km thick Voltaian Supergroup is considered analogous to the sedimentary rocks of the Taoudeni basin (Fig. 1a; Affaton et al., 1980; Villeneuve and Cornée, 1994; Anani, 1999). Weak deformation, lithofacies, extensive borehole coverage, airborne radiometric and geochemical data allowed for the stratigraphic division of the Voltaian Supergroup in three unconformable units, from bottom to top: Bombouaka, Oti, and Obosum groups (Table 1 and Fig. 2; Deynoux et al., 2006; Carney et al., 2010; Kalsbeek and Frei, 2010).

The Bombouaka Group comprises two sandstone-dominated units, which are separated by a middle mudstone unit. The rocks of the Bombouaka Group are interpreted as passive margin units of the Pharusian Ocean from lithofacies and geochemical studies (Kalsbeek et al., 2008; Anani et al., 2017). The WAC was inferred to be the source of the Bombouaka Group sediments (Anani, 1999; Anani et al., 2013, based on sandstone petrology and geochemical data), but Kalsbeek et al. (2008) and Anani et al. (2017) have inferred a significant contribution of sediments from the Amazonian Craton, based on geochemical data and U-Pb detrital zircon age fractions between 1700 and 1000 Ma, which are missing on the WAC but are abundant on the Amazonian Craton.

The Oti Group lies, with a glacial unconformity, on the Bombouaka Group, or locally, directly on the WAC basement rocks. The Oti Group comprises the Kodjari-Buipe and the Afram-Bimbila subgroups (Carney et al., 2010). The Kodjari-Buipe Subgroup corresponds to a "Triad" of glaciogenic deposits, baryte-bearing dolomitic limestone, and thinly bedded siliceous shale (Affaton, 1990;). The Afram-Bimbila Subgroup is composed of a rhythmic alternation of shale and siltstone, with various sandstone or greywacke interlayers, and lenses of clayey limestone. The depositional setting of the Kodjari-Buipe Subgroup is considered to be a passive margin of the Pharusian Ocean, based

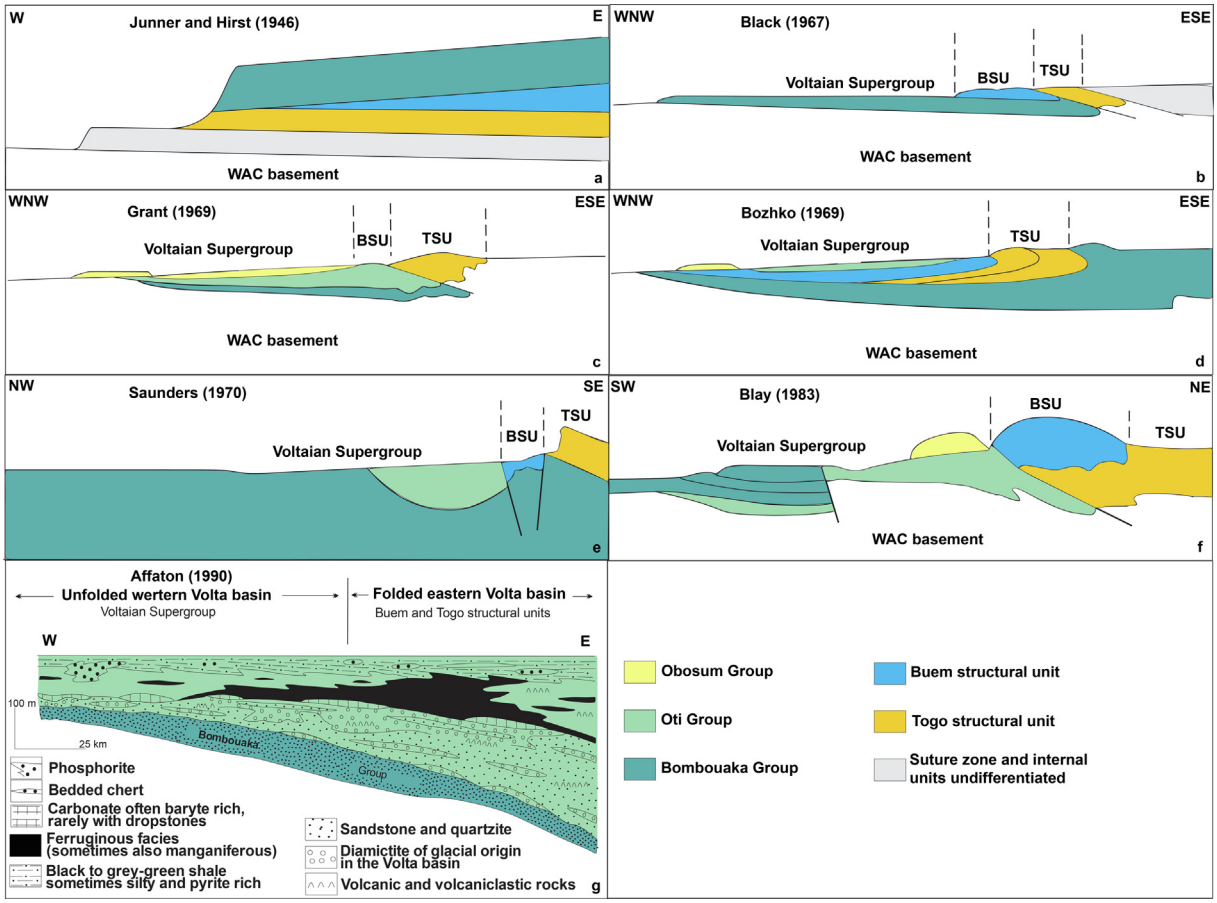

Fig. 4. The subdivisions and correlations of the Voltaian Supergroup, the Buem structural unit (BSU) and the Togo structural unit (TSU) proposed by (a) Junner and Hirst (1946), (b) Black (1967), (c) Grant (1969), (d) Bozhko (1969), (e) Saunders (1970), (f) Blay (1983), and (g) Affaton (1990).

on lithofacies and geochemical composition (Affaton, 1990; Carney et al., 2010; Amedjoe et al., 2018). The depositional setting of the Afram-Bimbila Subgroup is interpreted to be a peripheral (lies on the lower plate) foreland basin, based on the asymmetrical, wedge-like geometry that are typical of foreland basins (Jordan, 1981) and a significant proportion of detrital zircons in the age range between 900 and 600 Ma (Carney et al., 2010; Ganade de Araujo et al., 2016). The Afram-Bimbila Subgroup has been interpreted as flysch-derived (argillaceous sediments with rhythmic repetition of shale and siltstone) deposits from the Dahomeyide belt (Carney et al., 2010).

The Obosum Group is interpreted as a foreland basin molasse-type deposit, deposited at the late stage of the Pan-African continental collision (Carney et al., 2010; Kalsbeek and Frei, 2010). The Obosum Group is subdivided into the Yendi and Kebia subgroups (Table 1). The Yendi Subgroup includes a lower polymictic, micaceous and mainly sandy interval, overlain by a thick sequence of shale, impure limestone, and siltstone. The Kebia Subgroup is composed of various polymictic sandstone and conglomerate units, with lenses of shale and siltstone (Carney et al., 2010).

The Voltaian Supergroup was therefore deposited in two distinct depositional settings at different times. The Bombouaka Group and the Kodjari-Buipe Subgroup were deposited in passive margins at 959 ± 62 Ma (Rb-Sr isochrons on clay minerals) and ca. 635 Ma respectively (Table 1: Clauer, 1976; Carney et al., 2010). The depositional age of the Afram-Bimbila Subgroup is 576 ± 13 Ma (Lu-Hf dating on phosphorite; Barfod et al., 2004); however, the age of the Obosum Group is unknown, both deposited in a peripheral foreland basin.

The Neoproterozoic Togo structural unit (Fig. 2) consists of monocyclic arenaceous and argillaceous sedimentary rocks, which have been metamorphosed into quartzite, phyllite and schist (Junner and Hirst, 1946; Grant, 1969; Adjei and Tetteh, 1997). Anani et al. (2019) indicated that the geochemistry of the phyllite of the Togo structural unit signifies derivation from a passive continental margin. Detrital zircon age data suggest that the quartzite and schist (referred to as the Kanti schist) of the Togo structural unit were deposited in a passive margin and foreland basin respectively, with sediments sourced probably from the WAC-Amazonian Craton, and BNS respectively (Table 1; Kalsbeek et al., 2008; Ganade de Araujo et al., 2016).

The BSU, a fold and thrust belt, comprises dominantly shale and sandstone, and subordinate volcanic and mafic–ultramafic plutonic rocks, chert, carbonate, and ironstone (Fig. 5a; Ghana National Geological Mapping project, 2009; Kwayisi et al., 2020). Different workers have proposed different stratigraphic divisions for the BSU, because of intense folding and duplication by thrusting that obscure the original lithostratigraphic architecture (e.g., Supplementary Table S1 in Kwayisi et al., 2020). The BSU is deformed with generally steeply east-dipping S_2 foliation that is axial planar to near-isoclinal F_2 folds and local top-to-the west D_2 shear zones (Kwayisi et al., 2020), similar to the Togo structural unit (Agyei and Tetteh, 1997). The D_2 fabrics have locally been overprinted by D_3 deformation expressed as F_3 kink bands and open folds, with NE plunging fold axes (Kwayisi et al., 2020). From detailed fieldwork and petrographic studies, interpretation of airborne geophysical data, and qualitative restoration of orogenic structures, Kwayisi et al. (2020) produced a new map of the BSU in Ghana (Fig. 5a). This map reveals the occurrence of the ultramafic (mainly serpen-

Table 1
Compilation of available lithological, age, and depositional setting data on the Voltaian Supergroup, the Buem and Togo structural units.

Unit			Deposit type	Youngest zircon U-Pb age	Depositional age	Provenance
Voltaian Supergroup	Obosum Group	Kebia Subgroup Yendi Subgroup	Foreland (Molasse-type)[1,2]	591 Ma[1]	?	BNS[1,2]
	Oti Group	Afram-Bimbila Subgroup	Foreland (Flysch-type)[2,3]	600 Ma[2,3]	576 ± 13 Ma[4] (Lu/Hf, phosphorite)	BNS[3]
		Kojari-Buipe Subgroup	Passive margin[2,5]		ca. 635 Ma[2] (constrained by U-Pb zircon age of Marinoan glaciation event)	WAC[5] Amazonian Craton and WAC[1]
	Bombouaka Group		Passive margin [1,2,3,6,7,8]	1100 Ma[1]	959 ± 62 Ma[9] (Rb/Sr, clay fractions)	WAC[6,7] Amazonian Craton and WAC[1,8]
Buem structural unit	Uppermost		Foreland[3]	600 Ma[3]	ca. 650 Ma[11] (Rb/Sr, glauconite)	BNS[3]
	Upper and lower		Passive margin [1,3,10]	950 Ma[1]		WAC[10] Amazonian Craton and WAC[1]
Togo structural unit	Kanti schist Quartzite and phyllite		Foreland[3] Passive margin[1,3,12]	600 Ma[3] 950 Ma[1,3]	703 ± 8 Ma[13] (U-Pb zircon, metabasalt)	BNS[3] Amazonian Craton and WAC[2,12]

[1] Kalsbeek et al. (2008), [2]Carney et al. (2010), [3]Ganade de Araujo et al. (2016), [4]Barfod et al. (2004), [5]Amedjoe et al. (2018), [6]Anani (1999), [7]Anani et al. (2013), [8]Anani et al. (2017), [9]Clauer (1976), [10]Osae et al. (2006), [11]Clauer et al. (1982), [12]Anani et al. (2019), [13]Ganade de Araujo et al. (2014c).

tinised peridotite) rocks in top-to-the west thrust zones, which mark major tectonic contacts: to the west between the BSU and Voltaian Supergroup and the east between the BSU and Togo structural unit and within the sedimentary rocks of the BSU. It also led to an updated tectonostratigraphic division of the BSU into lower clastic units, followed by an ultramafic complex that is capped by chemical sedimentary units (chert and carbonate). These are overlain by gabbro and intermediate to mafic volcanic rocks, which are in turn overlain by the chemical units. The top part of the sequence consists of the upper clastic unit (Fig. 5b). All contacts between units are tectonic, expect for thin (3 m-thick) chemical units capping the ultramafic rocks, and gabbro locally in intrusive contact with volcanic rocks. Two main groups of sedimentary rocks have been identified in the BSU based on petrographic and geochemical data, and detrital zircon age fractions of the sediments; passive margin and foreland deposits (Table 1; Kalsbeek et al., 2008; Ganade de Araujo et al., 2016).

3. Field relations and petrography

Sedimentary rocks dominate the study area, occupying nearly 70% of the BSU (Fig. 5a). The sedimentary rocks of the BSU can be grouped into clastic and chemical units (Fig. 5b). The clastic units are sandstone, shale, turbiditic shale and diamictite, occupying the bottom and upper parts of the BSU, with the mafic–ultramafic and chemical units in the middle. The lower clastic units are overlain in thrust contact by the mafic–ultramafic rocks, whereas the upper clastic units make up the top of the tectonostratigraphic column. Figs. 6 and 7 illustrate the field and petrographic characteristics of the BSU clastic units respectively. The lower clastic units have undergone weak metamorphism defined by albite, quartz and muscovite and related to the ubiquitous D_2 deformation event described by Kwayisi et al. (2020). The upper clastic units are generally unmetamorphosed. The lower clastic units are largely fine- to medium-grained, consisting of intercalated quartzite and slate (Fig. 6a), usually occupying low topographical levels (forming lowlands). The lower clastic units are abundant in the eastern part of the study area, towards the contact with the Togo structural unit. The upper clastic units, on the other hand, consist generally of massive units (Fig. 6b) that occupy higher topographic levels (forming high ridges) than the lower clastic units, and consist of thick beds of well- to poorly-sorted units including diamictite, sandstone and shale (Fig. 6b and 6c). They are dominant in the western part of the study area, towards the contact with the Voltaian Supergroup.

The features of the framework grains of the BSU clastic units, characterised by abundant quartz, appreciable amounts of feldspar (plagioclase and K-feldspar) together with lithic fragments (volcanic rocks, slate, sandstone, greywacke, schist), classify them as quartz arenite, sublitharenite, subarkose, lithic subarkose and litharenite (diamictite) (Fig. 8). The main criterion for distinguishing lower and upper clastic units' quartz arenites is that the lower clastic units are bedded whereas the upper clastic units are generally massive. The shales vary in colour, ranging from dark grey, red, purple, green, to creamy white. The shales are grouped into upper shale and lower shale based on their position in the tectonostratigraphy (Fig. 5b). The upper shales occur as interbeds within the upper clastic units, while the lower shales occur within the lower clastic units.

3.1. Lower clastic units

The lower clastic units of the BSU are quartz-arenite (quartzite; NTDK3) and shales (slate; lower shale, NTDK124B and NTDK242B). The quartz arenite is thickly to thinly bedded, fine- to medium-

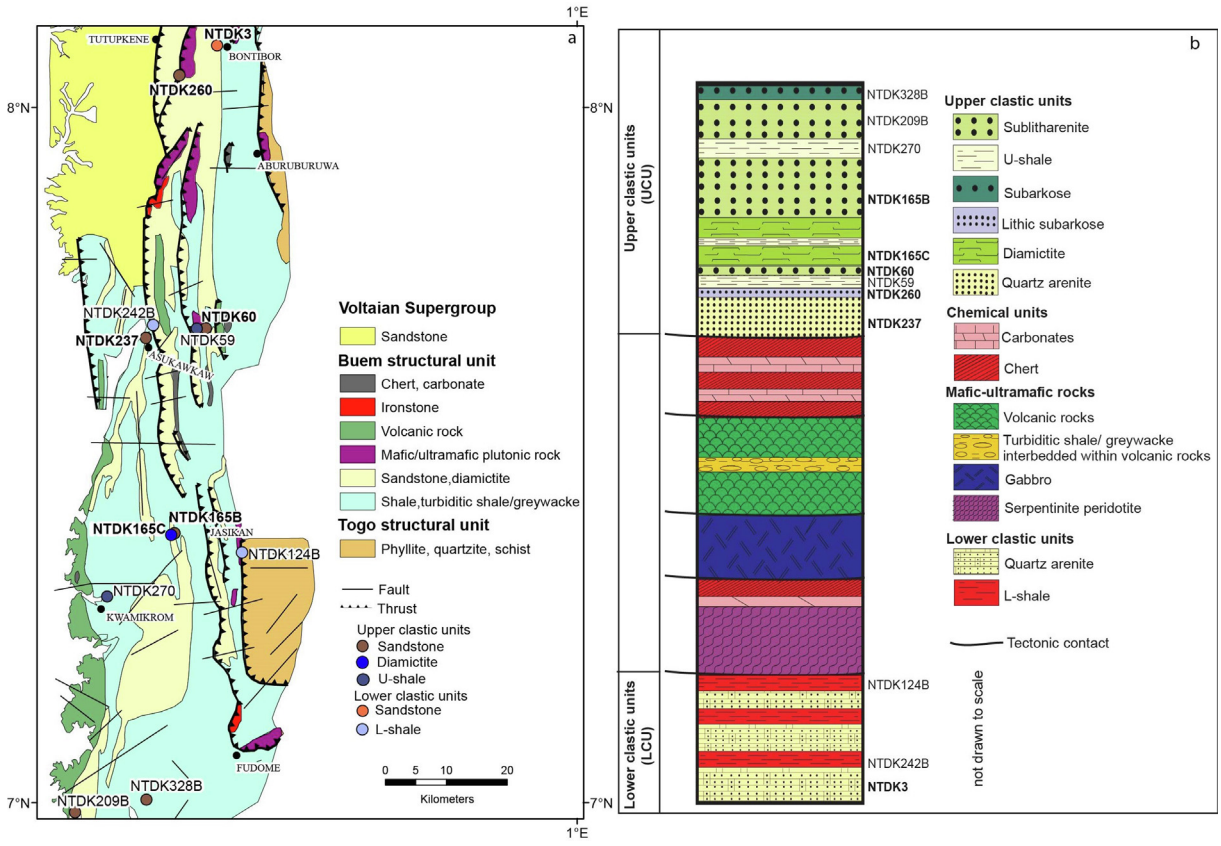

Fig. 5. (a) Geological map of the Buem structural unit, and (b) tectono-stratigraphic sequence of the Buem structural unit, showing structural relationships (modified from Kwayisi et al., 2020). Locations of new samples for geochemistry and U-Pb dating (bold) are shown in the map and stratigraphy.

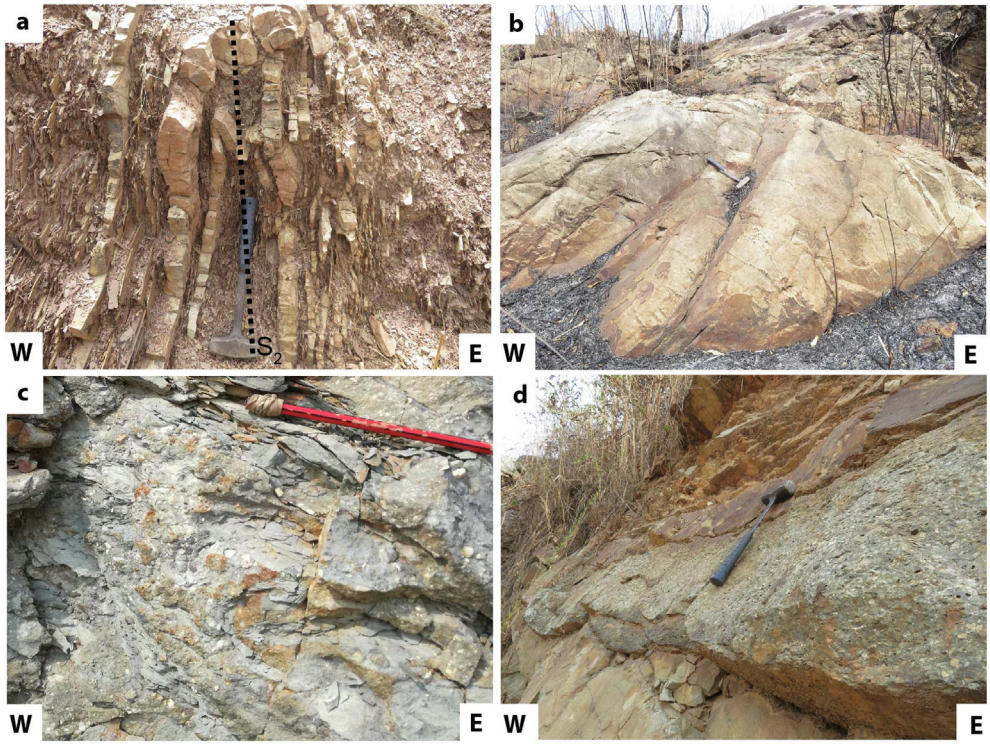

Fig. 6. Representative field photographs of the BSU clastic units shown in Fig. 3b. (a) Intercalation of quartz arenite and shale at the base of the BSU, (b) thickly bedded sandstone of the upper clastic units, (c) diamictite, and (d) thick beds of sandstone with diamictite interbed.

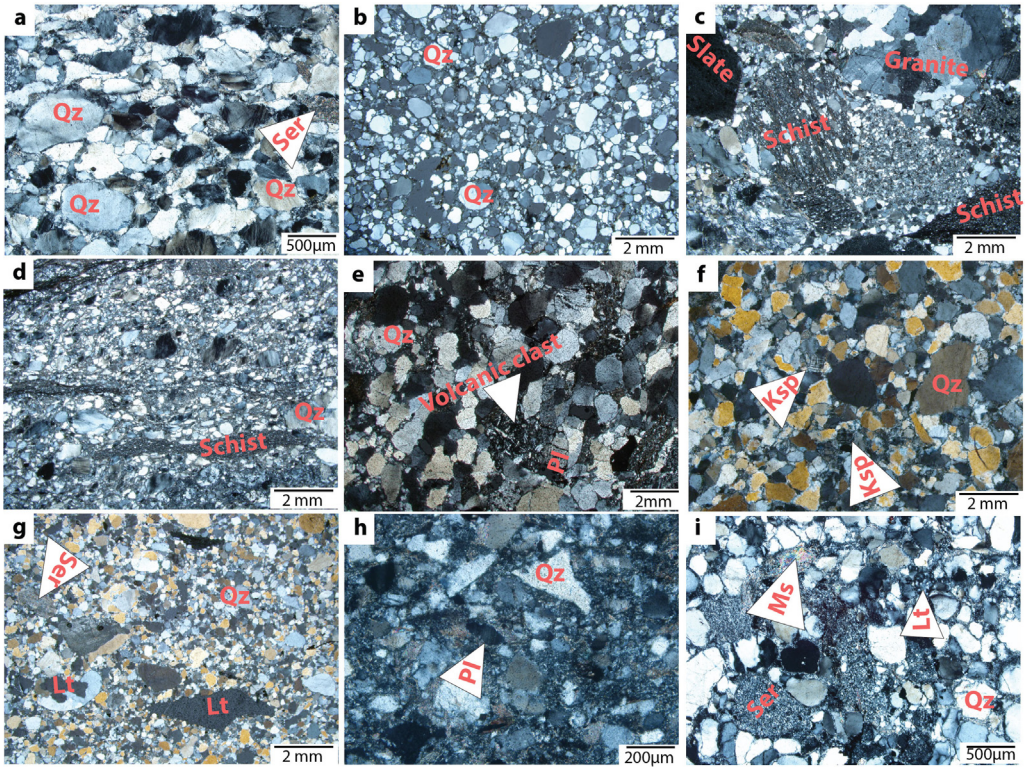

Fig. 7. Photomicrographs of (a) deformed quartz arenite at the base of the BSU showing elongated grains, (b) quartz arenite from the UCU, (c) diamictite, (d) deformed diamictite showing elongated clasts of schist, defining the S_2 slaty cleavage, (e) sublitharenite with volcanic clast and moderately- to well-sorted grains, (f) moderately sorted sublitharenite, (g) poorly-sorted sublitharenite, (h) subarkose with angular and poorly-sorted grains, (i) lithic subarkose showing significantly altered feldspars into sericite. Qz = Quartz, Ksp = K-feldspar, Pl = Plagioclase, Ser = Sericite (from Whitney and Evans, 2010) and Lt = Total lithic fragment (including polycrystalline quartz; after Dickinson et al., 1983).

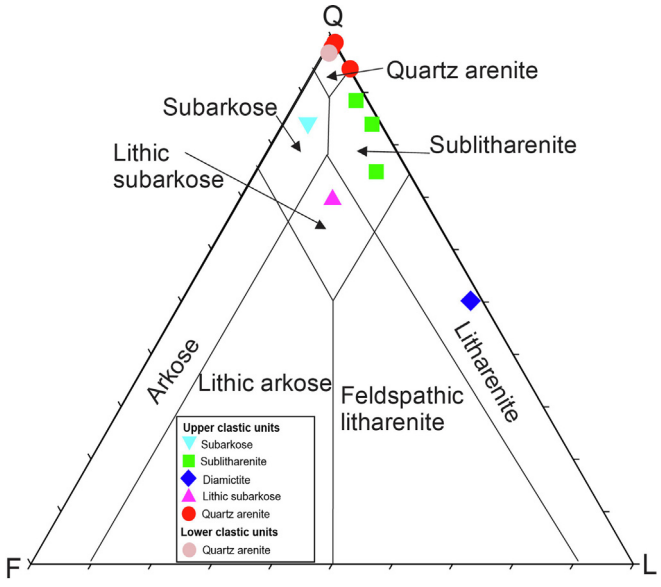

Fig. 8. QFL diagram (Dickinson et al., 1983) for the Buem sandstones and diamictite Q = quartz, F = feldspar, and L = lithic fragment (excluding polycrystalline quartz).

grained with sub-rounded to rounded clasts (Fig. 7a). It is composed of about 94 – 96% quartz grains, 1 – 3% lithic fragments (quartzite), 1 – 2% K-feldspar, and 1% muscovite (Fig. 7a). The framework grains of the quartz arenite are cemented mainly with silica. The quartz grains show undulose extinction and deformation lamellae. The K-feldspar is significantly altered to sericite. The lower shales are fine-grained, laminated and composed dominantly of clay minerals. They are intercalated with the quartz arenite (Fig. 6a). Lower shales seldom are in tectonic contact with the mafic–ultramafic plutonic rocks.

3.2. Upper clastic units

The upper clastic units include quartz arenite (NTDK237), diamictite or litharenite (NTDK165C), sublitharenite (NTDK60, NTDK165B, NTDK209B), subarkose (NTDK328B), lithic subarkose (NTDK269), and U-shale (NTDK59, NTDK270). The quartz arenite is generally massive, medium-grained, moderately- to well-sorted with sub-rounded to rounded grains (Fig. 6b and Fig. 7b). Framework grains in the quartz arenite are dominantly quartz (96 – 98%), and minor K-feldspar (2 – 4%), which are mainly cemented with silica. The diamictite occurs as massive beds that have coarse-grained (>2 mm) clasts embedded in fine-grained sand or clay matrix (Fig. 6c and d, and Fig. 7c). It is poorly sorted with sub-angular to rounded clasts. In a few samples, the grains are elongated and show a slightly preferred orientation (Fig. 7d). The diamictite is composed of quartz (45 – 55%), rock fragments (35 – 50%), plagioclase (1 – 2%), and muscovite (<1%). Rock fragments are clasts of schist (garnet-staurolite, biotite, quartz-sericite, and chlorite-quartz schist), slate, granite, greywacke, and volcanic material (Fig. 7c). The diamictite contains a sericite matrix and silica cement.

Three varieties of sublitharenites can be distinguished, based on texture and composition. Sample NTDK209 is medium to coarse-grained, moderate- to well-sorted with sub-rounded clasts (Fig. 7e). It is composed of quartz (75%), lithic fragments (15%

Table 2
Major and trace elements composition of the Buem sedimentary rocks. *Sandstone.*

Sample Id	NTDK3	NTDK237	NTDK60	NTDK209B	NTDK165B	NTDK165C	NTDK260	NTDK328B
Longitude	**0.489**	**0.3864**	**0.4771**	**0.2790**	**0.4292**	**0.4160**	**0.4342**	**0.3840**
Latitude	**8.092**	**7.6553**	**7.6811**	**6.9880**	**7.3751**	**7.3800**	**8.0422**	**7.0023**
	LOWER CLASTIC UNIT	**UPPER CLASTIC UNIT**						
	Quartz arenite		**Sublitharenite**			**Diamictite**	**Lithic subarkose**	**Subarkose**
SiO_2	92.88	96.3	92.38	73.98	79.44	95.55	89.5	74.14
TiO_2	0.19	0.12	0.16	0.56	0.33	0.12	0.17	0.68
Al_2O_3	3.44	1.81	3.7	11.51	9.02	2.7	4.59	10.66
Fe_2O_3	1.76	0.55	1.27	4.37	3.74	0.5	2.72	4.69
MnO	0.04	0.05	0.04	0.08	0.18	0.4	0.4	0.07
MgO	0.26	0.12	0.26	1.51	1.15	0.11	0.21	1.6
CaO	0.04	0.05	0.04	0.68	0.24	0.04	0.04	0.96
Na_2O	0.12	0.09	0.04	3.63	1.73	0.4	0.04	1.7
K_2O	0.49	0.4	1.13	1.35	2.11	0.74	1.04	2.05
P_2O_5	0.04	0.05	0.4	0.14	0.08	0.4	0.4	0.16
LOI	0.74	0.72	0.96	1.85	1.71	0.74	1.3	2.73
Sum	99.88	100.26	99.85	99.71	99.74	100.46	99.52	99.43
CIA	78	69	66	59	60	60	72	61
Sc	3.3	0.3	3.2	12	8.5	1.9	4.7	14
V	33	28	29	87	55	22	30	83
Co	1.5	0.6	3.4	9	14.5	0.5	4.7	12.2
Ni	12	7	11	22	28	4	10	38
Rb	22	4	47	39	72	27	45	92
Sr	30	1	0	136	91	5	16	63
Y	6.5	2.6	8.2	24.9	13.2	5.8	12.2	39.8
Zr	42	24	77	103	99	57	95	202
Nb	2.24	0.61	2.79	6.34	4.45	1.92	2.7	12.26
Cs	0.65	0.05	1.82	0.94	3.11	0.43	0.98	2.91
Ba	153	10	190	561	428	181	178	341
La	15.7	3.7	9.4	17.8	13.6	7.2	14.2	39.6
Ce	28.5	6.9	22.3	35.0	29.6	13.6	27.7	67.7
Pr	3.39	0.82	2.24	4.63	3.52	1.59	3.46	9.3
Nd	12.0	2.8	8.1	17.7	13.4	5.7	12.7	34.7
Sm	2.15	0.52	1.41	3.8	2.56	1.1	2.36	7.08
Eu	0.48	0.09	0.29	0.86	0.56	0.23	0.5	1.41
Gd	1.76	0.4	1.28	3.66	2.26	1.02	2.14	6.5
Tb	0.23	0.06	0.19	0.58	0.32	0.15	0.33	0.94
Dy	1.16	0.36	1.25	3.63	1.97	0.88	2	5.51
Ho	0.23	0.08	0.26	0.76	0.41	0.18	0.39	1.09
Er	0.60	0.20	0.79	2.25	1.23	0.49	1.04	2.93
Tm	0.09	0.03	0.13	0.33	0.18	0.07	0.17	0.42
Yb	0.57	0.23	0.87	2.26	1.21	0.49	1.13	2.82
Lu	0.08	0.03	0.15	0.34	0.19	0.08	0.17	0.44
Hf	1.2	0.69	2.2	2.83	2.74	1.63	2.64	5.73
Ta	0.18	0.04	0.2	0.47	0.34	0.15	0.2	0.86
Pb	3.64	0.96	3.79	9.72	11.21	5.17	11.13	16.47
Th	1.92	0.74	3.04	4.59	4.18	1.88	3.34	10.88
U	0.51	0.22	0.52	1.13	0.82	0.42	0.59	2.35
Eu/Eu*	0.75	0.59	0.67	0.70	0.71	0.66	0.68	0.64

Shale

Sample Id	NTDK59	NTDK270	NTDK124B	NTDK242B
Longitude	**0.4754**	**0.3240**	**0.5112**	**0.3991**
Latitude	**7.6782**	**7.2860**	**7.3574**	**7.6945**
	U-Shale		**L-Shale**	
SiO_2	69.02	68.98	62.98	69.52
TiO_2	0.63	0.63	0.78	0.66
Al_2O_3	15	14.99	16.46	11.84
Fe_2O_3	6.23	6.22	7.11	8.51
MnO	0.04	0.4	0.08	0.05
MgO	0.64	0.65	2.54	1.77
CaO	0.04	0.04	0.31	0.27
Na_2O	0.04	0.04	1.59	2.09
K_2O	3.72	3.72	4.15	2.71
P_2O_5	0.11	0.11	0.16	0.17
LOI	4.09	4.01	3.57	2.06
Sum	99.54	99.42	99.8	99.66
CIA	72	72	64	61
Sc	11	15	20	16
V	91	96	90	82
Co	14	14.2	17.9	8.9
Ni	38	39	189	26

(*continued on next page*)

Table 2 (*continued*)

Shale				
Sample Id	**NTDK59**	**NTDK270**	**NTDK124B**	**NTDK242B**
Longitude	**0.4754**	**0.3240**	**0.5112**	**0.3991**
Latitude	**7.6782**	**7.2860**	**7.3574**	**7.6945**
	U-Shale		**L-Shale**	
Rb	79	111	176	124
Sr	18	30	14	19
Y	9.6	16.8	36.6	33.8
Zr	139	138	159	245
Nb	8.72	8.84	13.88	23.33
Cs	6.25	6.06	6.36	4.09
Ba	884	919	590	175
La	6.8	20.6	14.5	30.3
Ce	36.4	47.1	59.9	63.2
Pr	1.92	5.36	3.86	7.6
Nd	7.4	19.5	14.7	28.1
Sm	1.64	3.7	3.61	5.61
Eu	0.44	0.91	0.82	1.09
Gd	1.82	3.38	3.9	5.11
Tb	0.31	0.5	0.67	0.83
Dy	1.89	2.92	4.56	5.25
Ho	0.4	0.61	1.02	1.08
Er	1.25	1.74	3.14	3.18
Tm	0.19	0.27	0.48	0.49
Yb	1.35	1.8	3.12	3.33
Lu	0.21	0.29	0.51	0.52
Hf	4	3.88	4.52	6.49
Ta	0.65	0.63	0.97	1.4
Pb	2.14	2.66	18.54	14.65
Th	4.23	5.34	12.17	11.79
U	1.42	1.5	2.04	1.89
Eu/Eu*	0.78	0.79	0.67	0.62

LOI = loss on ignition, CIA = chemical index of alteration, and ICV = index of compositional variability. The diamictite show very high SiO_2 content probably because most of the rock fragments and matrix are of silica-rich materials (Fig. 6c and d).

mainly volcanic clast), and plagioclase (10%). Sample NTDK60 is fine to medium-grained, moderately sorted with subangular to subrounded clasts (Fig. 7f). It is composed of quartz (85%), lithic fragments (8%) and K-feldspar (7%). Sample NTDK165B contains clasts ranging from fine to coarse-grained (Fig. 7g). It is poorly sorted and contains sub-angular to subrounded clasts. The framework grains of NTDK165B are quartz (84%), lithic fragments (14%), and K-feldspar (2%). The lithic fragments are sandstone and slate. Matrix content in the sublitharenites varies from 2 to 4% and is mainly sericite. The subarkose (NTDK328B) is generally poorly to moderately sorted and contains fine-grained angular clasts with abundant matrix (Fig. 7h).

The subarkose is quartz- and K-feldspar-dominated, making up 84% and 10% respectively of the total framework grains. Matrix content is about 6%. The K-feldspar is significantly altered to sericite. The lithic subarkose is medium-grained (NTDK260, Fig. 7i). Texturally, the lithic subarkose contains sub-angular to subrounded grains that are moderately sorted and slightly elongated. It is composed of quartz (70%), K-feldspar (12%) and lithic fragments (16%). K-feldspar is significantly altered to sericite. A significant amount of muscovite (2%) and trace amounts of zircon are observed. The matrix content of the lithic subarkose is about 2 – 5% and generally composed of sericite that is deformed between framework grains. Generally, the upper shales are fine-grained, laminated and composed dominantly of clay minerals. Thin layers of upper shale commonly occur as interbeds within the diamictite and the sublitharenite (Fig. 5b).

4. Sampling strategy and analytical techniques

To determine the depositional setting and potential provenance, 12 fresh and representative samples (each sample represent one sample block) of the BSU sedimentary rocks were analysed for their whole-rock major and trace element concentrations at the Spectrum Analytical Facility, University of Johannesburg, South Africa. Major and trace elements analyses were done by XRF spectrometer (Philips Panalytical MagiX Pro) and ICP-MS (Perkin Elmer NexION 300D) respectively. Their position in the stratigraphy is reported in Fig. 5b. Three samples from the lower clastic units include a quartz arenite (NTDK3) and two intercalated lower shales (NTDK124B, and NTDK242B). Nine samples were selected from the upper clastic units. They include one basal quartz arenite (NTDK237), three sublitharenites (NTDK60, NTDK165B, and NTDK209B), one diamictite (NTDK165C), one subarkose (NTDK328B), one lithic subarkose (NTDK260) and two upper shales interlayered with the sublitharenite (NTDK59 and NTDK270). Six samples of siliciclastic rocks, in stratigraphic order: NTDK3, and NTDK237, NTDK60, NTDK260, NTDK165C, and NTDK165B were selected for zircon U-Pb and Lu-Hf- analyses. The multi-collector inductively coupled plasma mass spectrometer (MC-ICP-MS; Nu Plasma II instrument) was used for the U-Pb and Hf analyses at the University of Johannesburg, South Africa. A detailed description of sample preparation and analytical procedure and protocol can be found in Supplementary Data A. The following parameters were used in calculating the epsilon-Hf (εHf(t)) and T_{DM} model age; a decay constant of 1.867×10^{-11} (Söderlund et al., 2004), depleted mantle values of $^{176}Hf/^{177}Hf$ = 0.28325 and $^{176}Lu/^{177}Hf$ = 0.0388 (Griffin et al., 2004), and CHUR parameters $^{176}Lu/^{177}Hf$ = 0.0336, $^{176}Hf/^{177}Hf$ = 0.282785 of Bouvier et al. (2008). The one-stage Hf model ages (T_{DM1}), calculated from the $^{176}Lu/^{177}Hf$ and $^{176}Hf/^{177}Hf$ ratios measured for the zircons of the BSU samples, can only give a minimum age for the proto-source material of the magma from which the zircon crystallised. Therefore, for each zircon, a two-stage Hf model age (T_{DM2}), or a "crustal" model age (T^{C}_{DM}), which assumes that its

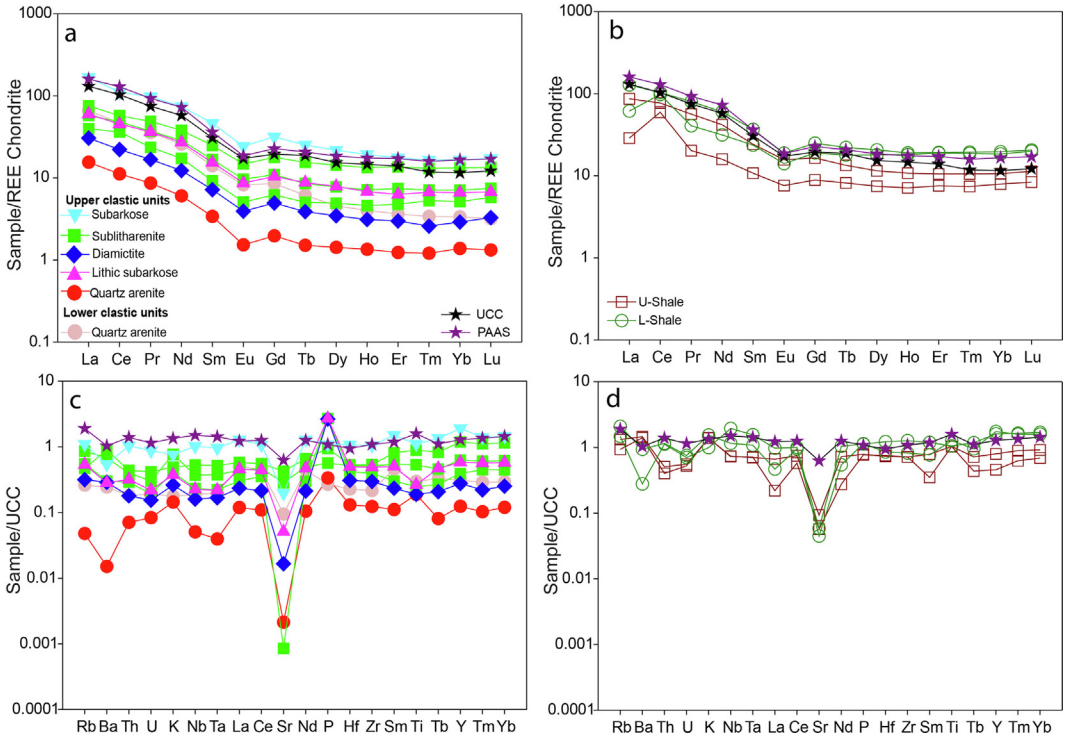

Fig. 9. Chondrite-normalized REE plot for (a) Buem sandstones and diamictite, (b) Buem shales. Multi-elements plot normalized to UCC (c) Buem sandstones and diamictite, and (d) Buem shales. Normalising values for UCC from Rudnick and Gao (2003) and chondrite from Taylor and McLennan (1985). PAAS is from McLennan (1989).

parental magma was produced from average continental crust ($^{176}Lu/^{177}Hf$ = 0.015; Griffin et al., 2004) that originally was derived from the depleted mantle, was calculated.

5. Major element and trace element characteristics

Table 2 presents the whole-rock major and trace element concentrations of the sedimentary rocks of the BSU. Post-diagenetic alteration and metamorphism can affect the concentration of the major elements, especially MgO, CaO, Na_2O and K_2O, and increase the volatile content, as measured by the loss on ignition (LOI) of sedimentary rocks (Jiang et al., 2017). Therefore, it is important to evaluate the influence of post-diagenetic alteration and metamorphism on the mobility of the elements on the BSU sedimentary rocks. All the samples of the BSU have low LOI content (0.7 – 4.1 wt %), which makes it less likely that significant remobilisation of these major elements has occurred during post-diagenetic alteration and metamorphism.

The chemical index of alteration (CIA) permits the assessment of the intensity of chemical weathering at the source of the sedimentary rocks, particularly the conversion of feldspars to clay minerals (Nesbitt and Young, 1982). The CIA is defined by the molar ratio $[Al_2O_3/(Al_2O_3 + CaO^* + Na_2O + K_2O)]/100$, with CaO^* signifying Ca in the silicate fraction i.e. exclusive of calcite, dolomite and apatite ($CaO^* = CaO - CO_2$ (cc) – (0.5 × CO_2 (dol)) − 10/3 (P_2O_5) (ap)) (Nesbitt and Young, 1982). In this expression, cc is calcite, dol is dolomite and ap is apatite. McLennan (1993) indicated that in cases where CO_2 is not measured, the expression for CaO^* becomes $CaO^* = CaO$ − 10/3 (P_2O_5) (ap); we use this approach here, as CO_2 was not measured, and carbonates is not noted within thin sections. Low CIA (50) values show a weak intensity of weathering while high (∼100) values signify high chemical weathering (Nesbitt and Young, 1982). The CIA values calculated for the BSU sedimentary rocks vary between 69 and 78 for the quartz arenites and 59 to 66 for the sublitharenites. The diamictite, subarkose, and lithic subarkose respectively have CIA values of 60, 61 and 72 (Table 2). The shales have CIA values of 72 (upper shale), and 61–64 (lower shale). The CIA values for the BSU sedimentary rocks indicate low to moderate degrees of chemical weathering.

Because the Rare Earth Elements (REEs), High Field Strength Elements (HFSEs) and transition metals are least affected by post-depositional alteration and metamorphism (Taylor and McLennan, 1985; McLennan et al., 1993), potential provenance and depositional setting interpretations will be based on these elements only. The BSU sedimentary rocks exhibit similar REE patterns, comparable to Upper Continental Crust (UCC) and Post-Archean Australian Shale (PAAS), with concentrations of the Light REE (LREE) up to 100 times chondrite, nearly flat Heavy REE (HREE), and negative Eu anomalies on the chondrite-normalised REE diagram (Fig. 9a and 9b). Two of the shales show pronounced positive Ce anomalies. Fig. 9c and 9d are the diagrams of the incompatible trace element concentrations normalized to UCC for the BSU sedimentary rocks. On these diagrams, the BSU sedimentary rocks are similar to PAAS but display stronger Sr depletion (Fig. 9c). The diamictite, sublitharenites and lithic subarkose have positive K peaks although absolute values are lower than for PAAS and UCC. Upper clastic units' quartz arenite, sample NTDK237, has the lowest trace element concentration, showing a Nb-Ta trough, depletion in Ba, and enrichment in K, P and Ti. A very weak Nb-Ta trough is also evident for the lithic subarkose, diamictite, and two sublitharenite samples (NTDK60 and NTDK165B). The lithic subarkose, diamictite, and a sublitharenite (NTDK209B) exhibit a positive P anomaly. The overall trace element patterns for the shales resemble that of PAAS and the concentrations are almost the same as UCC (Fig. 9d).

6. Zircon morphology, U-Pb age distribution, and Lu-Hf isotope composition

Cathodoluminescence (CL) images of detrital zircon grains together with spot ages and εHf(t) values are given in Supplementary Data B and the U-Pb zircon analysis results for the samples of

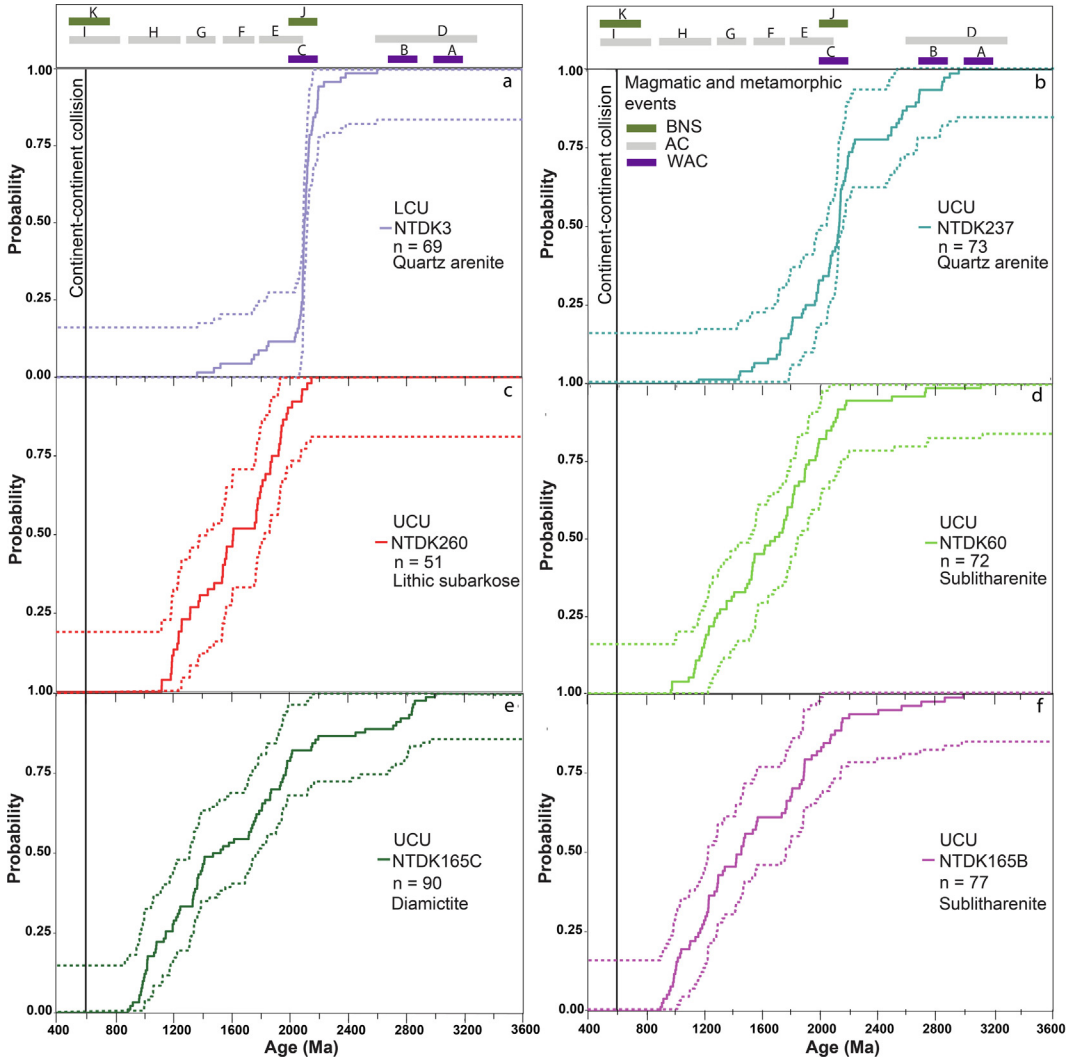

Fig. 10. Cumulative age distribution plots for near-concordant (10% discordance limit) zircons from the BSU samples. The letters A to K represent major magmatic and metamorphic events on the WAC (purple), BNS (green), and the Amazonian Craton (AC, grey). A = Leonian, B = Liberian, C = Eburnean, D = Archean events, E = Ventuary-Tapajós, F = Rio Negro-Juruena, G = Rondonian-San Ignacio, H = Sunsas-Aguapeí, I = Brasiliano, J = Paleoproterozoic basement, K = magmatism in the upper plate (i.e., BNS) during Pan-African plate convergence of the Dahomeyide belt. The dashed lines are the confidence intervals.

Table 3
Zircon age distributions of the Buem samples.

Sample	Classification	Position	Age fraction (Ma)	Percentage
NTDK165B	Sublitharenite	Top part of upper clastic unit	1650 – 900	61%
			2400 – 1740	34%
			2980 – 2560	5%
NTDK165C	Diamictite	Upper clastic unit	1590 – 890	54%
			2190 – 1620	33%
			2990 – 2450	13%
NTDK60	Sublitharenite	Upper clastic unit	1550 – 970	46%
			2150 – 1620	49%
			3110 – 2500	5%
NTDK260	Lithic subarkose	Upper clastic unit	1600 – 1130	48%
			2150 – 1700	52%
NTDK237	Quartz arenite	Lower part of the upper clastic unit	1550 – 1140	7%
			2240 – 1640	71%
			2960 – 2470	22%
NTDK3	Quartz arenite	Lower clastic unit	1530 – 1370	4%
			2350 – 1741	95%
			2600	1%

the BSU are available in Supplementary Data C. In this study, a total of 581 zircons were analysed in six BSU samples for their U-Pb ages, of which 432 analyses provided ages within ± 10% concordance and only these near-concordant data will be discussed. The reported U-Pb ages are $^{207}Pb/^{206}Pb$ ages, although $^{235}U/^{206}Pb$ ages are shown in Supplementary Data C. The Lu-Hf isotope compositions for the near-concordant zircons from the BSU samples are given in Supplementary Data D. The results are illustrated in the cumulative age distribution (Fig. 10), probability density and kernel density estimate plots (Supplementary Data E). The results are presented in stratigraphic order, starting with the lowermost sample as shown in Fig. 5b.

The zircons separated from sample NTDK3 (quartz arenite) collected within the lower clastic units, generally have regular oscillatory or sector zoning, and mostly exhibit rounded grain morphologies. The zircons have 1:1 to 2:1 length to width ratios and range between 55 and 160 μm in size. They dominantly have Th/U ratios between 0.3 and 1.0 with very few grains having Th/U ratios of 0.08 – 0.27. The dominant $^{207}Pb/^{206}Pb$ age fraction is 2350 – 1740 Ma (95%), with two zircon grains at 1530 and 1370 Ma (4%) and one single 2600 Ma (1%) zircon grain for the 69 near-concordant zircons analysed for this sample (Table 3). Most of the zircon grains in this sample are between 2200 and 2040 Ma (Fig. 10a, and Supplementary Data E), with a peak at 2100 Ma.

The initial $^{176}Hf/^{177}Hf$ isotopic ratios of this sample vary from 0.28100 to 0.28191. The Paleoproterozoic zircon grains gave negative and positive εHf(t) values from −14.4 to + 8.6, with the majority in the range −5 to + 5 (Fig. 11a) corresponding to Hf crustal model ages (T^C_{DM}) from 3.6 to 2.2 Ga (Supplementary Data D). The two zircons of Mesoproterozoic age have positive εHf(t) values close to + 3 and Hf crustal model ages of ca. 2.1 Ga.

The quartz arenite at the base of the upper clastic unit (Fig. 5b), sample NTDK237, predominantly contains rounded zircon grains that are mostly zoned (oscillatory zoning) and have a length to width ratios of 1:1 to 2:1 and size of 80 to 160 μm. Th/U ratios of these zircons are mainly between 0.3 and 2.0, with few grains between 0.2 and 0.3. The 73 near-concordant zircons analysed from this sample yielded a prominent zircon $^{207}Pb/^{206}Pb$ age fraction of 2240 – 1640 Ma (71%), with a dominant fraction of 2240 – 1900 and a peak at 2150 Ma (Table 3, Fig. 10b, and Supplementary Data E). Minor amounts of zircon with ages of 2960 – 2470 Ma (22%) and 1550 – 1170 Ma (7%) are also recorded.

This quartz arenite sample records a wider range of initial $^{176}Hf/^{177}Hf$ isotopic ratios of 0.28047 – 0.28195 than sample NTDK3. The zircon grains with Archean ages have εHf(t) values of + 1.1 to −17.2 and Hf T^C_{DM} of 4.3 – 3.0 Ga (Supplementary Data D). Paleoproterozoic and Mesoproterozoic zircon grains yielded negative and positive εHf(t) values, −20.0 to + 4.3 and −4.3 to + 3.0 respectively (Fig. 11a), corresponding to Hf T^C_{DM} ages = 3.9 – 2.4 Ga and 2.4 – 2.0 Ga, respectively.

Sample NTDK260 (lithic subarkose), which conformably overlies quartz arenite sample NTDK237, contains dominantly euhedral and a few rounded zircons, which display internal zoning. The zircons range in size from 60 to 100 μm and have between 1:1 and 2:1 length to width ratios. These zircon grains have Th/U ratios of mostly 0.3 – 2.0 and minor 0.07 – 0.30. Sample NTDK260 mainly contains zircons of 2150 – 1700 Ma (52%) (with two peaks, at 1950 Ma and 1800 Ma), and of 1600 – 1130 Ma (48%) (with peaks

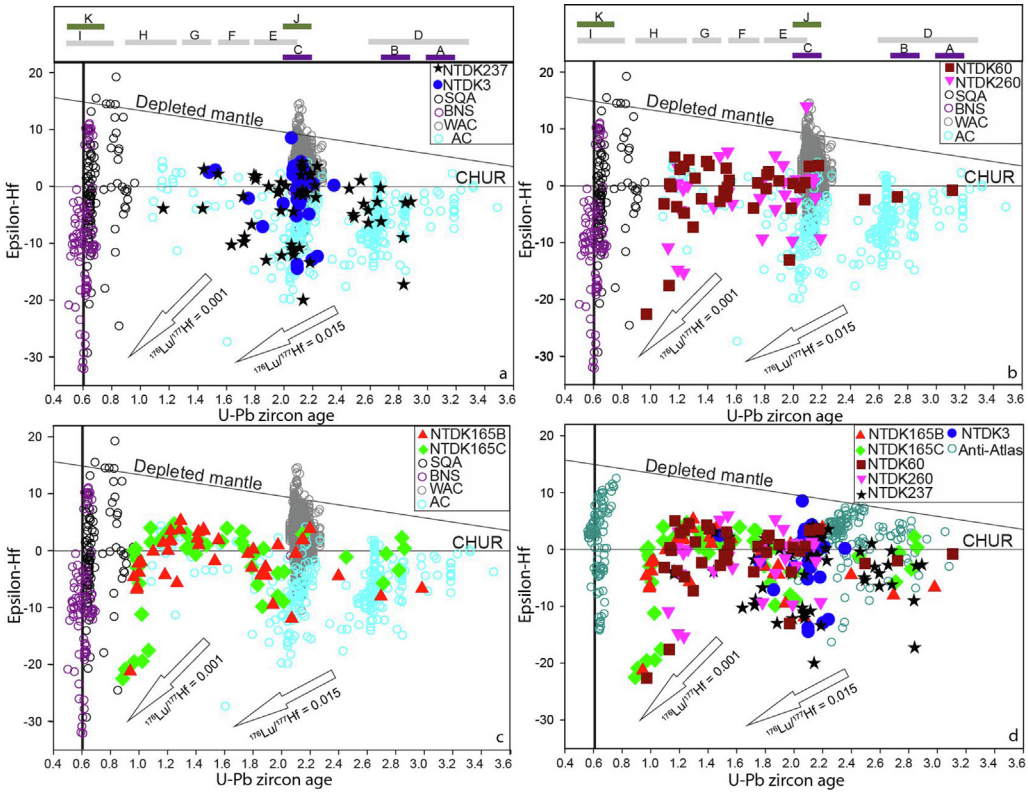

Fig. 11. Epsilon-Hf vs. age diagram for the Buem samples, showing the detrital zircon data relative to CHUR and Depleted Mantle evolution curves and comparison to published data for the WAC, BNS, AC and the Santa Quitéria Arc (SQA), (a) samples NDTK3 and NTDK237, (b) samples NTDK60 and NTDK260, (c) samples NTDK165B and NTDK165C, (d) comparison of the BSU samples with the Neoproterozoic Pan-African Anti-Atlas belt in Morocco. Published data are from Parra-Avila et al. (2017) and Peterson et al. (2018) for the WAC, Pepper et al. (2016), Neto and Lofan (2019) for the AC, Ganade de Araujo et al. (2016) and Kalsbeek et al. (2020) for the BNS, Ganade de Araujo et al. (2014b) for SQA, and Abati et al. (2012) for Anti-Atlas belt. The letters A to K represent major magmatic and metamorphic events on the WAC, BNS, and the Amazonian Craton.

at 1550 Ma and 1200 Ma) (Table 3, Fig. 10c, and Supplementary Data E).

In terms of Hf isotopic composition, this sample shows a wide range of initial $^{176}Hf/^{177}Hf$ isotopic ratios (0.28112 – 0.28212), with positive and negative εHf(t) values of −9.7 to + 5.3 (Paleoproterozoic grains) and −15.3 to + 6.0 (Mesoproterozoic grains) (Fig. 11b). Hf crustal model ages for the Paleoproterozoic and Mesoproterozoic zircon grains are 3.5 – 2.3 Ga, and 3.1 – 1.9 Ga, respectively (Supplementary Data D).

Sample NTDK60 (sublitharenite) conformably overlies sample NTDK260 and is separated from it by a shale layer. Zircons separated from sample NTDK60 generally have regular internal zoning, exhibiting both euhedral and rounded grain morphologies. The zircons have 1:1 to 2:1 length to width ratios and range between 70 and 150 μm in size. They have Th/U ratios dominantly between 0.3 and 1.7 with very few grains having Th/U ratios of 0.1 – 0.3. Sample NTDK60 contains zircon $^{207}Pb/^{206}Pb$ age fractions in the ranges 3110 – 2500 Ma (5%), 2150 – 1620 Ma (49%), and 1550 – 970 Ma (46%) from the 72 near-concordant zircons analysed (Table 3, and Fig. 10d).

Initial $^{176}Hf/^{177}Hf$ of this sample range between 0.28075 and 0.28218 with the following εHf(t) values and Hf crustal model ages for the various zircon age fractions: −0.8 to −2.4 and T^{C}_{DM} = 3.6 – 3.2 Ga for Archean zircons, −13.0 to + 3.6 and T^{C}_{DM} = 3.4 – 2.3 Ga for Paleoproterozoic zircons, −17.6 to + 5.1 and T^{C}_{DM} = 3.1 – 1.7 Ga for Mesoproterozoic zircons, and –22.6 and T^{C}_{DM} = 3.2 Ga for the one Neoproterozoic zircon grain analysed (Fig. 11b, Supplementary Data D).

The diamictite sample (NTDK165C) that conformably overlies the sublitharenite (NTDK60) has the largest zircon grains (100–230 μm) compared to the other samples. The zircon grains are mostly internally zoned and predominantly of rounded morphology. The zircon grains have Th/U ratios predominantly in the range 0.3 – 2.0 and subordinately 0.01 – 0.30. Zircon $^{207}Pb/^{206}Pb$ age fractions recorded from the 90 near-concordant analysed zircons are, from least to most prominent: 2990 – 2450 Ma (13%), 2190 – 1620 (33%), and 1590 – 890 Ma (53%), (Table 3, and Fig. 10e).

The initial $^{176}Hf/^{177}Hf$ isotopic ratios of the zircons vary from 0.28158 to 0.28095. The εHf(t) values and depleted mantle extraction ages are −5.7 to + 2.3 and T^{C}_{DM} = 3.5 – 3.1 Ga for Archean zircons; −9.8 to + 3.9 and T^{C}_{DM} = 3.2 – 2.2 Ga for Paleoproterozoic zircons; −19.4 to + 4.7 and T^{C}_{DM} = 3.0 – 1.7 Ga for Mesoproterozoic zircons; and –22.5 to + 0.4 and T^{C}_{DM} = 3.0 – 1.8 Ga for the Neoproterozoic zircons (Fig. 11c, and Supplementary Data D).

The sublitharenite, sample NTDK165B, conformably overlying the diamictite (NTDK165C) with a stratigraphic contact, contains both rounded and euhedral zircon grains that are mostly zoned (oscillatory zoning) and have a length to width ratios of 1:1 to 2:1 and sizes of 70 to 230 μm. Th/U ratios of these zircons are mainly between 0.3 and 2.0, with few grains between 0.04 and 0.30. The 77 near-concordant zircons analysed from this sample yielded zircons $^{207}Pb/^{206}Pb$ age fractions at 2980 – 2560 Ma (5%), 2400 – 1740 Ma (34%), and 1650 – 900 Ma (61%) (Table 3, Fig. 10f, and Supplementary Data E).

In terms of Hf isotopic composition, this sample yielded initial $^{176}Hf/^{177}Hf$ isotopic ratios of 0.28067 – 0.25211. Hf model ages for Archean grains are T^{C}_{DM} = 4.0 – 3.7 Ga with mainly negative εHf(t) values from −8.0 to −6.7 (Supplementary Data D, Fig. 11c). Hf model ages for Paleoproterozoic and Mesoproterozoic zircon grains respectively vary from T^{C}_{DM} = 3.4 – 2.5 Ga, and 2.7 – 1.8 Ga and both positive and negative εHf(t) values of −11.9 to + 3.8 (Paleoproterozoic grains) and −3.7 to + 5.3 (Mesoproterozoic grains). Neoproterozoic zircon grains have mainly negative εHf(t) values (-21.3 to −4.7) and Hf model ages of T^{C}_{DM} = 3.1 – 2.1 Ga. Summary of the petrographic, geochemical, and geochronological characteristics of the BSU sedimentary rocks are shown in Supplementary Data F.

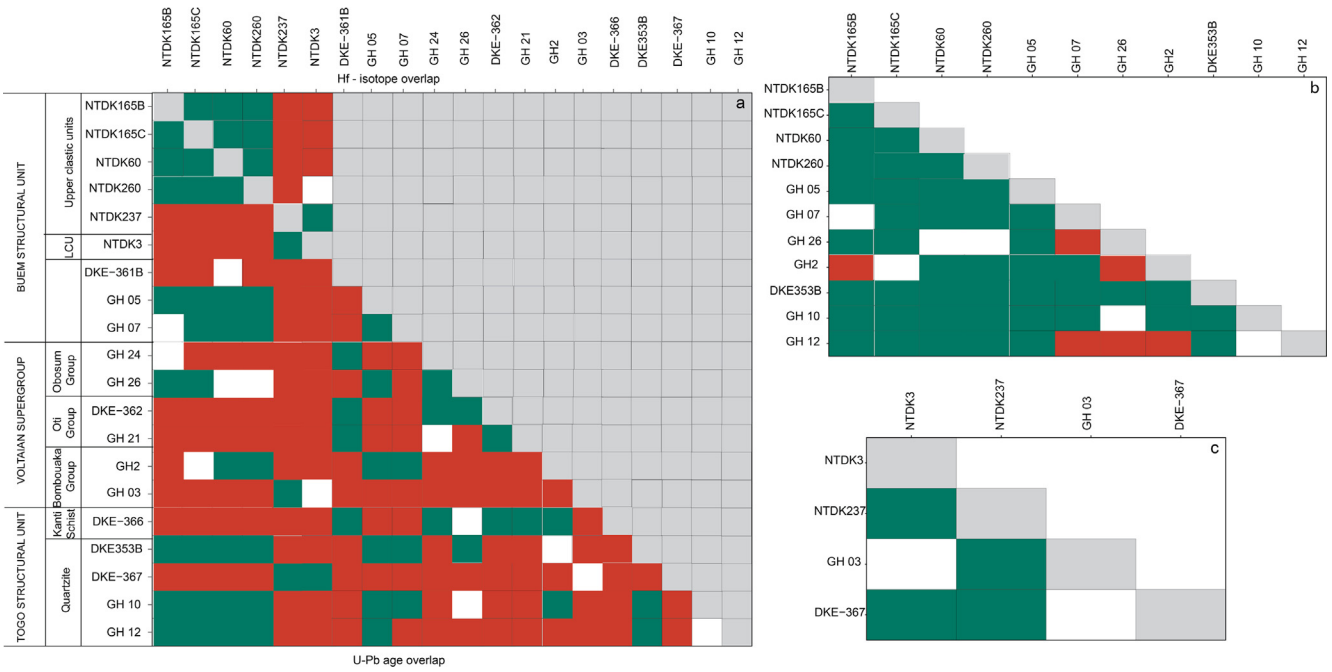

Fig. 12. (a) Pairwise comparison of the confidence intervals of zircon U-Pb age distributions and Hf-in zircon isotopic composition among the individual samples of the BSU and with published data, using the 1-O parameter of Andersen et al. (2016) as a measure of difference. Note the upper part of the plot is Hf-in zircon comparison while the lower part is for U-Pb age, (b) Pairwise comparison of the upper clastic units of the BSU showing extensive similarity to the Bombouaka Group, and the quartzite of the TSU, and (c) Pairwise comparison of the lower clastic unit and the lower part of the upper clastic units of the BSU showing extensive similarity to Bombouaka Group and the quartzite of the TSU. Green = 0 (statistically indistinguishable at the 95% confidence level), white = 0–0.05, red = >0.05 (statistically different), and grey = no data. LCU = Lower clastic units. Published data are from Kalsbeek et al. (2008) and Ganade de Araujo et al. (2016).

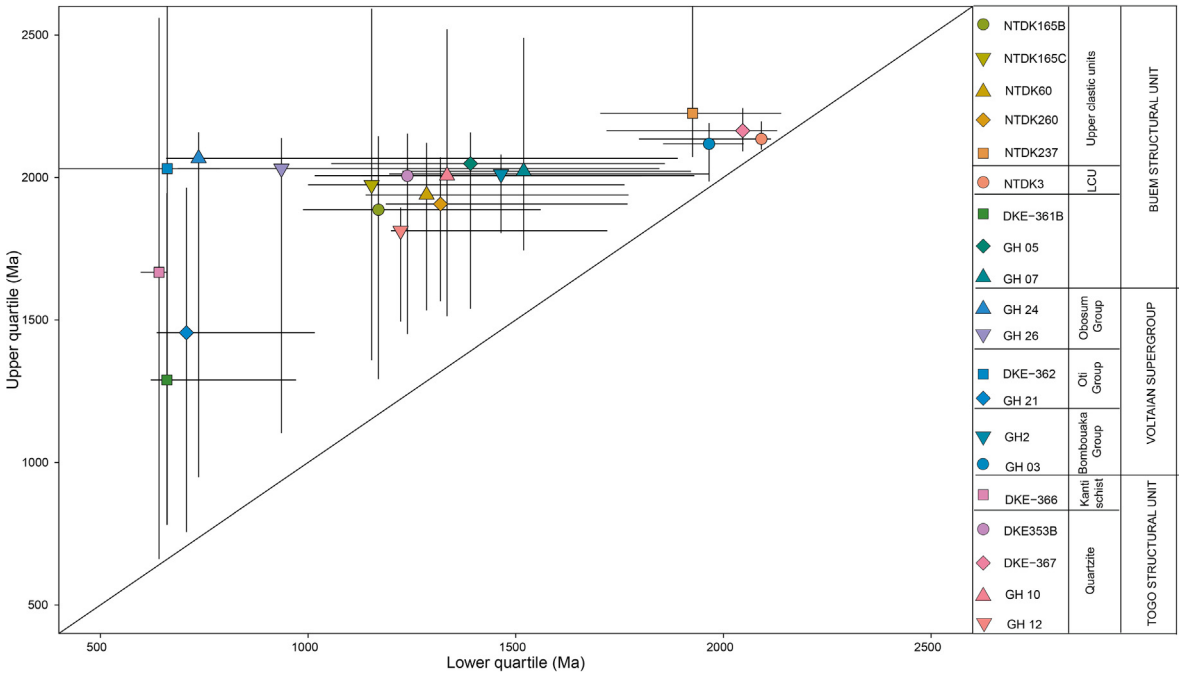

Fig. 13. Upper quartile vs. lower quartile plots, after Andersen et al. (2018), of zircon U-Pb age data for the BSU samples and published data. Published data are from Kalsbeek et al. (2008) and Ganade de Araujo et al. (2016). The orthogonal lines on each sample point are confidence limit (2 sigma).

7. Discussion

7.1. Tectonostratigraphic record of the BSU

A first-order examination of the cumulative age distribution curves and the U-Pb detrital zircon age vs. εHf(t) patterns in Figs. 10 and 11 allows us to distinguish three main provenance signatures within the BSU: 1. Samples NDTK3 and NTDK237, from the base of the lower and upper clastic units respectively, contain prominent 2300 – 1800 Ma (60 – 89%) zircons.; 2. Samples NTDK60 and NTDK260, in the upper clastic units, contain predominantly 1800 – 1100 Ma (64 – 67%) zircons and a minor fraction at 2300 – 1800 (35%), but lack Neoproterozoic zircons grains; 3. Samples NTDK165B and NTDK165C, occupying the top part of the upper clastic units, contain a significant fraction of Neoproterozoic grains (1000–970 Ma, 7%). Some of the 1200 – 900 Ma zircons from the upper clastic units with pronounced negative εHf(t) values between −10 and −23 and T^{C}_{DM} model ages between 3.1 and 2.5 Ga are arranged in a linear array with a slope of $^{176}Lu/^{177}Hf$ of ~0.001 (Fig. 11b and c). This suggests the main phase of crustal growth between 3.1 and 2.5 Ga and subsequent resetting of the U-Pb system during the early Neoproterozoic. Some of these late Mesoproterozoic and Neoproterozoic zircons, however, show juvenile characteristics, having εHf(t) values of + 5.3 to 0 (Fig. 11b and c).

As a measure of similarity between samples, the 1-O method as proposed by Andersen et al. (2016) was employed because it takes the uncertainty on the distribution into account. Where O represents the part of the cumulative age distribution curve over which the confidence intervals of the two samples overlap ($0 \leq O \leq 1$). O = 1.0 signifies that the samples have indistinguishable age distribution patterns (Andersen et al., 2016). The pairwise O values for the samples from the BSU are shown in Supplementary Data G, and Fig. 12 represents a graph of 1-O illustrating the similarity pattern of the BSU samples. On the graph, the two lowermost samples NTDK3 and NTDK237 are consistently distinct from the other samples of the BSU. The Lower Quartile (LQ) vs Upper Quartile (UQ) plot (Fig. 13) reinforces that samples NTDK3 and NTDK237 are similar by having a narrow age (2100 – 1800 Ma) distribution of their zircons, which is significantly different from the other samples (from 900 to 1800 Ma).

Although from Figs. 12 and 13 samples NTDK165B and NTDK165C, and samples NTDK260 and NTDK60 are undistinguishable, only samples, NTDK165B and NTDK165C, contain Neoproterozoic zircons with only moderately negative εHf(t) values of −1 to −5. It is thus clear that three broad groups of samples exist within the BSU, those with older age fractions dominantly 2300 – 1800 Ma, represented by samples from the lower clastic units and base of the upper clastic units, those with prominent 1800 – 1100 Ma zircons occupying the middle part of the upper clastic units, and those with significant 1000 – 970 Ma age fractions, forming the uppermost part of the upper clastic units of the BSU.

7.2. Depositional setting

7.2.1. Maturity and recycling of the sediments

There is a large variation in texture and mineralogical content observed for the siliciclastic rocks of the BSU. This calls for an investigation on the maturity of the sediments, using joint textural observations and chemical maturity indexes, such as Th/Sc and Zr/Sc. A plot of Th/Sc versus Zr/Sc is an important discriminator to differentiate between the contrasting effects of proto-source composition and sedimentary sorting or recycling on the composition of siliciclastic sedimentary rocks (McLennan et al., 1993). The BSU sedimentary rocks display wide variations in their Zr/Sc and Th/Sc ratios (Fig. 14a). Except for the quartz arenite at the base of the upper clastic units which plot far above UCC and PAAS, the other sandstone samples plot close to UCC and PAAS. This may reflect unrecycled upper continental crust material to intensely recycled detritus, suggestive of immature to mature sediments. All the BSU shale samples have Zr/Sc and Th/Sc ratios lower than UCC and PAAS, indicating that sedimentary recycling process was not pronounced in the shales and thus the shales are composed of immature sediments. The large variation in the Zr/Sc and

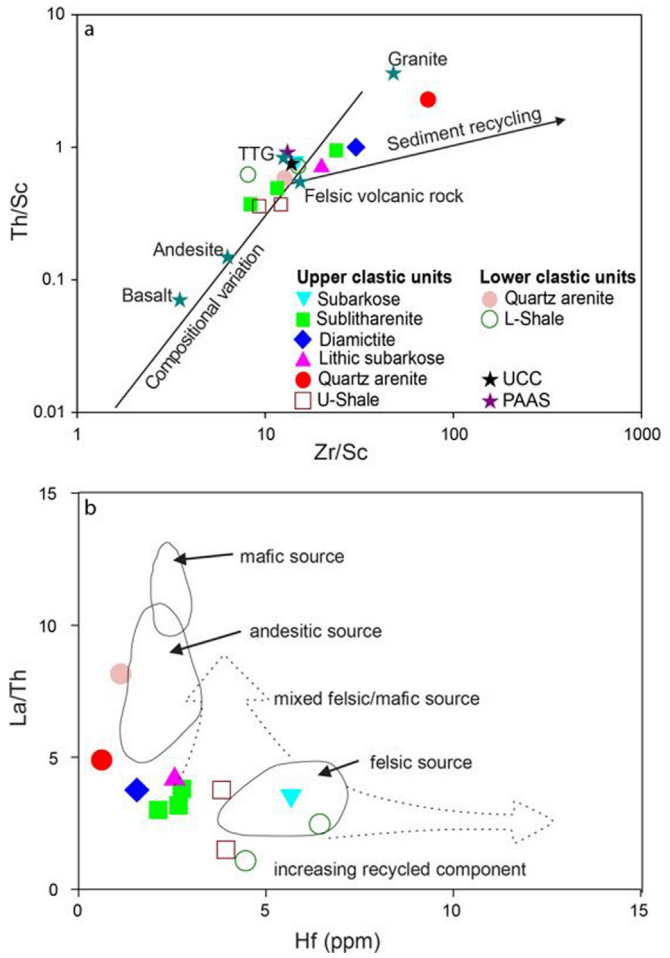

Fig. 14. (a) Th/Sc versus Zr/Sc after (McLennan et al., 1993). Note data points from TTG, granite, felsic volcanic rocks, andesite, and basalt are from Condie (1993), and (b) plot of La/Th against Hf for the BSU sedimentary rocks (composition fields after Floyd and Leveridge, 1987).

Th/Sc ratios exhibited by the BSU sedimentary rocks (Fig. 14a) may indicate poor mixing of the sediments in these rocks, a reflection of the intercalation of shale and sandstone within the lower clastic unit, and sandstones with shale interbeds within the upper clastic units (Fig. 5b).

7.2.2. Composition of the source area

The detrital zircons of the BSU sandstones and diamictite show a large range of U-Pb ages and Hf isotope model ages of 3110 – 970 Ma and 4.3 – 1.7 Ga respectively, a reflection of the accumulation of sediments from a mixture of young and old continental crust made up of juvenile mantle and reworked crustal materials or pre-existing sedimentary rocks. This, coupled with the fact that weathering and recycling rates do not follow stratigraphic succession, indicates the contribution of detritus to the sedimentary basin from different proto-sources (proximal and distal) of different emplacement ages or sediments thereof. Mafic igneous rocks usually have minimal negative Eu anomalies ($Eu/Eu^* = 0.8 – 1$), whereas negative Eu anomalies ($Eu/Eu^* = 0.5 – 0.8$) are often observed in felsic igneous rocks (Taylor and McLennan, 1985; Cullers, 1994; Cullers and Podkovyrov, 2000). Thus, the negative Eu anomalies shown by all the BSU sedimentary rocks may suggest the accumulation of detritus from felsic igneous rocks or sediments. The Th/Sc versus Zr/Sc ratios suggest that the BSU sedimentary rocks were sourced from mixed felsic and intermediate proto-source rocks of dominantly TTG and felsic volcanic rocks, with minor contributions from granite and/or andesite or sediments thereof (Fig. 14a). To further assess the composition of the BSU sedimentary rocks, the ratio of La/Th versus Hf content was employed. The low concentration of Hf with correspondingly low La/Th ratios in the BSU sedimentary rocks implies sediment derivation from an intermediate source rock plotting close to the mixed felsic/mafic source regions (Fig. 14b). Overall, the BSU sedimentary rocks were derived from mixed sources of felsic and intermediate source rocks.

7.2.3. Tectonic setting of the BSU sedimentary rocks

Two tectonic setting models have been proposed for the BSU sedimentary rocks. Osae et al. (2006) proposed a passive margin setting for the sandstones (upper and lower) of the BSU, based on petrography and major element composition. Kalsbeek et al. (2008) indicated that the sandstone for the upper and lower part of the BSU with passive margin geochemical characteristics have detrital zircon ages of 950 Ma and older. Foreland basin sedimentary rocks of the Dahomeyide belt are characterised by detrital zircon ages of 900 – 600 Ma (Kalsbeek et al., 2008; Ganade de Araujo et al., 2016). Thus, Ganade de Araujo et al. (2016) considered a foreland basin for the uppermost part of the BSU sandstones because of the significant amounts of detrital zircon grains with ages 900 – 600 Ma. Detrital zircon grains obtained from the BSU sandstones and diamictite yielded a wide range of ages from 3110 to 970 Ma. Youngest detrital zircon ages of passive and foreland sedimentary rocks of the Dahomeyide belt are at ca. 950 and 600 Ma respectively (Kalsbeek et al., 2008; Ganade de Araujo et al., 2016). Detrital zircons with ages between 1000 and 950 Ma constitute about 7% on average of the total zircons analysed from the BSU samples (this study). Thus, the absence of detrital zircons of ages between 900 and 600 Ma of the BSU sandstones (this study) may suggest their deposition in a passive margin depositional setting.

7.3. Correlations of the Buem structural unit with Voltaian Supergroup and Togo structural unit

The detrital zircon and geochemical record of the BSU is compared with the Voltaian Supergroup (Kalsbeek et al., 2008; Ganade de Araujo et al., 2016; Anani et al., 2017; Abu and Zongo, 2017; Amedjoe et al., 2018) and Togo structural unit (Kalsbeek et al., 2008; Ganade de Araujo et al., 2016; Anani et al., 2019). The quartzite of the Togo structural unit and Bombouaka Group of the Voltaian Supergroup have zircon age fractions of 2200 – 930 Ma and 2200 – 1130 Ma respectively (Figs. 12, 13, and 15a and b; Kalsbeek et al., 2008; Ganade de Araujo et al., 2016). Neoproterozoic zircon grains of 900 – 600 Ma have been recorded in the sandstones of the Oti and Obosum groups of the Voltaian Supergroup and the Kanti schist of the Togo structural unit (Figs. 12, 13, and 15c; Kalsbeek et al., 2008; Ganade de Araujo et al., 2016). The BSU has been divided into upper and lower sections by Affaton (1990), using a diamictite unit as a marker. Affaton (1990) suggested that the lower (below the diamictite) and upper (above the diamictite) sections of the BSU correlate with the Bombouaka and Oti groups, respectively.

Kalsbeek et al. (2008) inferred a possible correlation between the sandstones of the BSU with the Bombouaka Group and the quartzite of the TSU on the basis of detrital zircon ages of > 950 Ma obtained for the BSU sandstones. In this study, samples of the BSU contain detrital zircon with ages of ca. 970 Ma (upper clastic units) and 1130 Ma (lower clastic units) and older, similar to the quartzite of the Togo structural unit and Bombouaka Group respectively (Figs. 12, 13 and 15). The zircon age population from the BSU (this study) is however, distinct from the Oti and Obosum groups, and the Kanti schist (Figs. 12, 13 and 15). The absence of

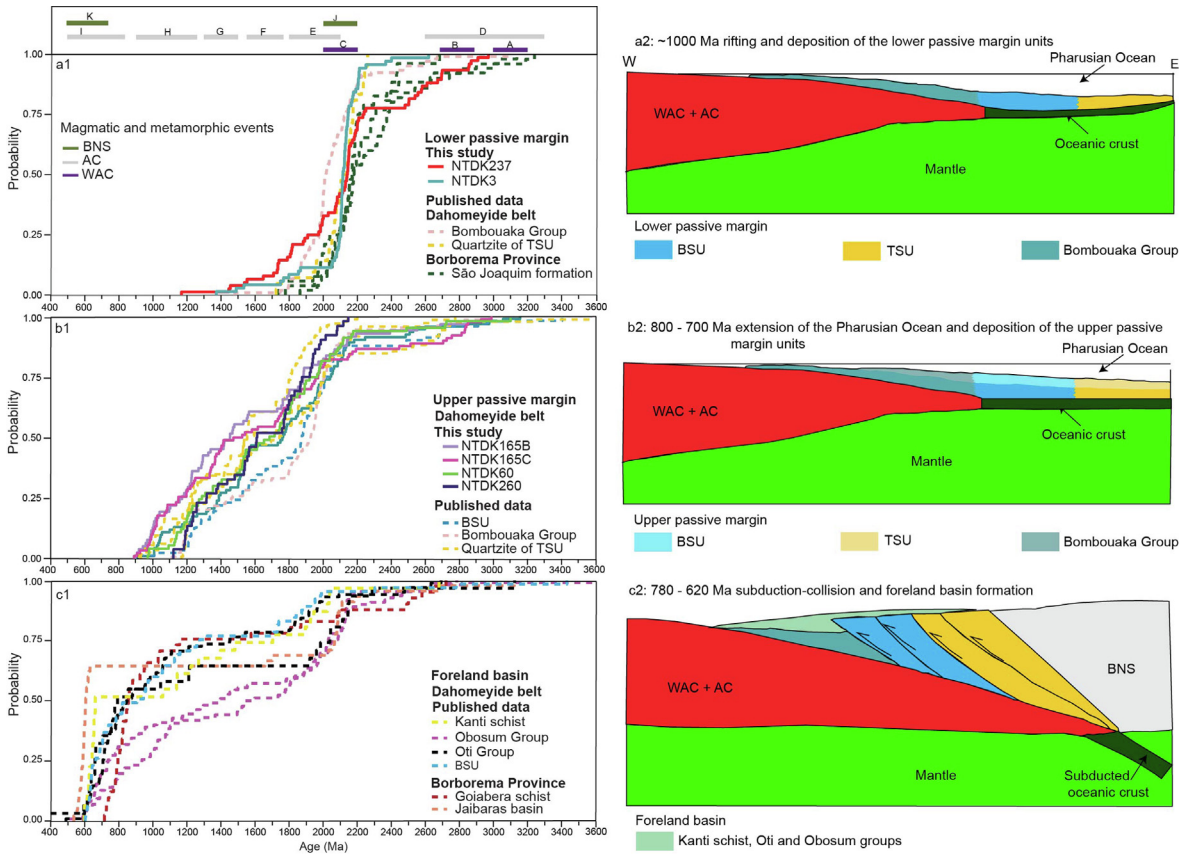

Fig. 15. Cumulative age distribution plots for the BSU samples compared to published data for the Voltaian Supergroup, TSU and BSU and correspond schematic diagram illustrating the geodynamic evolution of the external zone of the Dahomeyide belt. (a) Lower passive margin, (b) upper passive margin, and (c) foreland basin. Published data are from Kalsbeek et al. (2008) and Ganade de Araujo et al. (2012, 2016). The letters A to K represent major magmatic and metamorphic events on the WAC, BNS, and the AC, see Fig. 10 for details.

900 – 600 Ma zircon grains from the upper clastic units, even for the units above the diamictite (Fig. 5b; this study) may suggests that the upper section of the BSU in Ghana may not correlate with the Oti Group as suggested by Affaton (1990). However, zircons of such ages have been recorded for one sandstone sample (DKE-361B) of the upper part of the BSU in Benin (Fig. 2, Ganade de Araujo et al., 2016). The Benin sandstone (DKE-361B) is distinct from the sandstone samples analysed in this present study, as shown in Figs. 12 and 13, and may thus correspond to a part of the BSU that is missing from the stratigraphy of the Ghana section of the BSU, or it is yet to be sampled.

Based on geochemical composition and detrital zircon ages of > 950 Ma, Kalsbeek et al. (2008), Ganade de Araujo et al. (2016), Abu and Zongo (2017) and Anani et al. (2017; 2019) proposed that the Bombouaka Group and the Togo structural unit formed in the same passive margin basin of the Dahomeyide belt. Based on the youngest detrital zircon at 600 Ma, Ganade de Araujo et al. (2016) inferred a foreland (peripheral) basin setting for the Oti Group and Kanti schist. However, Amedjoe et al. (2018) considered the Oti Group to have been deposited in a passive margin setting, based on geochemical characteristics. Although some of the Oti samples have active margin signature, Amedjoe et al. (2018) interpreted that as inherited from an old island-arc source area, i.e. the WAC basement. Considering all the evidence, it is therefore proposed that the BSU, Togo structural unit and Bombouaka Group possibly formed in the same depositional basin, as reflected by similar geochemical features and detrital zircon age distributions.

7.4. Potential provenance of the BSU sedimentary rocks

Detrital zircons recognized to be of igneous origin can be used to determine major magmatic events in the proto-source areas (Condie et al., 2009), and obtain information regarding continental crust formation and evolution from their Lu-Hf isotopic composition (Andersen et al., 2016). A majority (>75%) of the zircons of the BSU sedimentary rocks have regular internal zoning (Supplementary Data B) with Th/U ratios between 0.3 and 2.0 (Supplementary Data C), in agreement with an igneous origin (e.g. Kinny et al., 1990; Hoskin and Schaltegger, 2003; Corfu et al., 2003). Thus, the U-Pb ages and Lu-Hf isotopic composition obtained from the igneous zircons of the BSU sedimentary rocks reflect the timing of their crystallisation, which in turn provides important constraints on the crustal evolutionary history of their proto-source.

A minor amount of 3110 – 2500 Ma (7%) zircons is recorded in most of the analysed samples of the BSU. All the samples from the BSU contain zircons in the age range from 2200 to 1800 Ma (33% – 93%). The potential sources for these zircons are the basement rocks of the WAC, Amazonian Craton, and/or the Benino-Nigerian Shield. The WAC is divided into a western Archean basement and eastern Paleoproterozoic domain; these two areas are characterised by greenstones, granitoids, and granitic gneisses of ages between 3500 and 2500 Ma, and between 2200 and 2000 Ma respectively (e.g. Abouchami et al., 1990; Taylor et al., 1992; Potrel et al., 1998; Egal et al., 2002; Sakyi et al., 2014; Anum et al., 2015; Kouamelan et al., 2015; Rollison et al., 2016; Grenholm et al., 2019) (Fig. 11). Metasedimentary rocks of Paleo-

proterozoic age (2200 – 1900 Ma) are associated with the Paleoproterozoic greenstones, granitoids and granitic gneisses. Also, Archean and Paleoproterozoic greenstones, granitoids and granitic gneisses (3500 – 1800 Ma) are exposed on the Amazonian Craton (Cordani et al., 2009; Neto and Lofan, 2019). Therefore, potential sources for the Archean and the Paleoproterozoic zircons of the BSU sedimentary rocks are the granitoids and granitic gneisses of the Archean and Paleoproterozoic basement and/or sedimentary rocks associated with the Paleoproterozoic granitoids and granitic gneisses of the WAC and the Amazonian Craton. Major and trace element concentrations of the BSU sedimentary rocks and the Hf isotopic ratios of their zircons indicate that they originated from a felsic/intermediate continental basement with minimal to intense sedimentary recycling.

The BSU has been reported to be underthrust by the Paleoproterozoic Birimian rocks based on field data (Attoh, 1998; Attoh and Nude, 2008) and processing of aeromagnetic data (Kwayisi et al., 2020). Additionally, the low positive and low to high negative εHf(t) values for the Archean and Paleoproterozoic zircons of the BSU sedimentary rocks are within the range for the Archean and Paleoproterozoic granitoids and sedimentary rocks of the WAC and more especially the Amazonian Craton (Fig. 11a to c; Parra-Avila et al., 2017; Pepper et al., 2016; Petersson et al., 2018; Neto and Lofan, 2019). The Benino-Nigerian Shield is a source area that could be considered as it consists of 2200 – 2000 Ma granitic gneisses and metasedimentary rocks (Attoh et al., 2013; Ganade de Araujo et al., 2016; Kalsbeek et al., 2020), which were reworked during the Pan-African orogeny (Attoh et al., 2013; Ganade de Araujo et al., 2016). However, this is considered unlikely because a signature of Benino-Nigerian Shield provenance is Pan-African zircons (900 – 600 Ma, Kalsbeek et al., 2008; Ganade de Araujo et al., 2016), which are absent in our samples (Figs. 11 and 15). Moreover, all paleogeographic reconstructions suggest that the WAC and Benino-Nigerian Shield were not attached until the assembly of Gondwana at ca. 500 Ma (Rogers and Santosh, 2002; Abdelsalam et al., 2002; Meert et al., 2012).

The WAC provenance does not explain our age fraction at 1700 – 1000 Ma, which is present in most of the BSU samples, because the WAC did not record any major tectono-metamorphic events between 1700 and 1000 Ma (Ennih and Liégeois, 2008). The proportion of zircons with ages of 1700 – 1000 Ma in the BSU samples varies with stratigraphic position, from bottom to top 9% (NTDK3), 18% (NTDK237), 64% (NTDK260), 55% (NTDK60), 54% (NTDK165C) and 56% (NTDK165B) (Table 3). Other peripheral basins to the WAC, such as the Neoproterozoic sedimentary rocks from the Pan-African Anti-Atlas belt, southern Morocco, lack detrital zircons of age fractions between 1700 and 800 Ma (Fig. 11d; Abati et al 2012), suggesting that this age fraction could be sourced from areas external to the WAC such as the Amazonian Craton.

Late Paleoproterozoic and Mesoproterozoic (1700 – 1000 Ma) granitoids and granitic gneisses are widespread on the Amazonian Craton (Fig. 11a to c; e.g. Santos et al., 2000, 2008; Tassinari et al., 2000; Cordani et al., 2009; Pepper et al., 2016). In the Rondonian–San Ignacio and Sunsas-Aguapeí belts of the Amazonian Craton (Fig. 1b), rocks of these ages are dominant (e.g., Sadowski and Bettencourt, 1996; Cordani and Teixeira, 2007). Besides recent paleogeography reconstruction of Rodinia from U-Pb baddeleyite ages and paleomagnetic data on dolerite dyke swarms put the Amazonian and West African cratons together (Baratoux et al., 2019; Antonio et al., 2021). The Amazonian Craton is positioned to the north of the WAC. This is consistent with paleocurrent data of Bombouaka sandstones which, indicates NW- and NE-directed sediment flow (Carney et al., 2010). Thus, the accumulation of greater proportions of the detritus into the BSU from the Amazonian Craton during Rodinia break-up is most likely. Moreover, the positive and negative εHf(t) values for the zircons with ages ranging from 1700 to 1000 Ma of the BSU samples are within the range for the granitoids and sedimentary rocks of similar ages within the Amazonian Craton (Fig. 11a to c; Pepper et al., 2016).

Kalsbeek et al. (2008) and Ganade de Araujo et al. (2016) have proposed an Amazonian Craton contribution to the sediment supply for the sandstones of the Bombouaka Group of the Voltaian Supergroup and the quartzite of the Togo structural unit based on detrital zircon age fraction of 1700 – 1000 Ma (Fig. 15). The Neoproterozoic rocks of the Taoudeni basin (Fig. 1a), which are correlative to the Voltaian Supergroup, also record detrital zircon with ages between 1700 and 1000 Ma, which have been interpreted to have been sourced probably from the Amazonian Craton (Straathof, 2011).

More recently, Kalsbeek et al. (2020) obtained a 1146 ± 4 Ma U-Pb zircon age from an augen-gneiss in contact (unclear the type of contact) with the quartzite of Togo structural unit to the east. Kalsbeek et al. (2020) inferred that this age could indicate a Mesoproterozoic magmatic event that has not yet been identified on the WAC, and thus this augen-gneiss could have contributed to the sediment supply to the sandstones of the Bombouaka Group, quartzite of the Togo structural unit and sandstones of the BSU. However, there is still the need to account for the detrital zircon age fractions between 1700 and 1300 Ma, 1000 and 900 Ma, and the pronounced negative εHf(t) values, between − 10 and − 20 of the 2200 – 1800 age fraction (Fig. 11), which are missing from the geological records of the WAC. Hence, the record of 1700 – 1000 Ma zircon age fractions in the BSU strengthens the Amazonian-WAC connection. Thus, during Rodinia time, the WAC and the Amazonian Craton were probably not separated by any major seas and these cratons may have been connected since the Paleoproterozoic until the breakup of Pangea as have been proposed by Rogers (1996), Trompette (1994), Rogers and Santosh (2002), and Evans (2009, 2013).

Neoproterozoic zircons are only recorded in the uppermost part of the UCU (NTDK165B and NTDK165C) of the BSU in low proportions (average 7%; Table 3). As discussed earlier, about 50% of these zircons (980 – 890 Ma), having εHf(t) values between − 10 and − 23 and T^{C}_{DM} model ages between 2.5 and 3.1 Ga may have lost Pb whereas only a few (990 – 970 Ma) show more juvenile characteristics, having εHf values of + 5.3 to 0. These few juvenile Neoproterozoic zircon grains could have been sourced from geological domains on the Amazonian Craton. Widespread over the Amazonian Craton is the 1000 – 970 Ma anorogenic granitoids which formed at the end of the Sunsas orogeny with comparable εHf(t) values (+7 to 0; Pepper et al., 2016). In addition, the Goais magmatic arc that provided 900 – 750 Ma detrital zircons to the passive margin sedimentary rocks in eastern Amazonia could be a possible source for these Neoproterozoic zircons (Fig. 11; Cordani and Teixeira, 2007; Pepper et al., 2016).

In a summary, the detrital U-Pb zircon ages and Lu-Hf isotope compositions of the BSU reveal the Amazonian Craton as the potential provenance for its sedimentary rocks with or without any contribution from the WAC.

7.5. Evolution of the external zone of the Dahomeyide belt

Results from this study, together with published data on the BSU, Togo structural unit and the Voltaian Supergroup, reveal two main sedimentary sequences in the external zone of the Dahomeyide belt, i.e., passive margin and foreland basin sequences with three potential provenances: Amazonian Craton, Benino-Nigerian Shield, ± WAC (Fig. 15; Kalsbeek et al, 2008; Ganade de Araujo et al., 2016; this study). The 3110 to 930 Ma zircon fraction correspond to an Amazonian Craton provenance, with a minor contribution from the WAC, whereas the 900 – 600 Ma is the signature of the Benino-Nigerian Shield provenance (Fig. 11 and Fig. 15). The

evolution of the passive margin sequence of the Dahomeyide belt started with the deposition of the Bombouaka Group (with depositional age at 959 ± 65 Ma from a Rb–Sr isochron on clay, Clauer, 1976). This was followed by the deposition of the Togo and Buem structural units (Fig. 15a), with depositional ages respectively at 703 ± 8 Ma (zircon U-Pb on a metavolcanic rock in the Togo structural unit; Ganade de Araujo et al., 2014a) and at ~ 650 Ma (Rb/Sr in glauconite on a shale unit in the BSU; Clauer, 1982 in Guillot et al., 2019). This large variation in depositional ages reflects a long period of passive margin basin existence (from ~ 1000 to ~ 700 Ma) (Fig. 15b; Ganade de Araujo et al., 2016, this study). Passive margin sedimentation was halted by the onset of the Neoproterozoic Pan-African orogeny, which resulted in subduction and collision between 750 and 570 Ma (Affaton et al., 2000; Hirdes and Davis, 2002; Guillot et al., 2019). Deposition of foreland basin sequences (Oti and Obosum groups and the Kanti schist) occurred during and after Pan-African continent–continent collision (Fig. 15c). First, there was the deposition of the Kodjari-Buipe Subgroup of the Oti Group with a ~ 635 Ma (Marinoan glaciation) depositional age. Second, the Afram-Bimbila Subgroup of the Oti Group and the Kanti schist were deposited, based on the 600 Ma youngest detrital zircon age. The final one to be deposited was the Obosum Group, which overlies the Afram-Bimbila Subgroup, and which has a maximum depositional age of ~ 591 Ma, based on the youngest detrital zircon (Ganade de Araujo et al., 2016).

7.6. Implications for the paleogeographic reconstruction of the West African and Amazonian cratons in Rodinia

Passive margin units consisting of pre- and syn- to post-rift metasedimentary rocks occur in the Pharusian belt, the northern segment of the WGO (Caby, 2014). Although no radiogenic isotope nor geochronological data are available on these passive margin units, their deposition may have occurred before 790 Ma, which is the age of an intra-oceanic arc gabbro (793 – 790 U-Pb zircon ages) that intruded them (Caby, 2014). In the Borborema Province, which is the southeastern segment of the WGO, the sedimentary rocks of the Martinópole Group show similar detrital zircon age distribution, depositional settings, and provenance patterns (Fig. 1b; Ganade de Araujo et al., 2012) as the external zone of the Dahomeyide belt (Fig. 15). The São Joaquim Formation of the Martinópole Group was deposited in a passive margin (Fig. 15a), with a depositional age of 777 Ma (U-Pb zircon age of interleaved felsic volcanic rocks) and sediments sourced from the Amazonian Craton and WAC (Ganade de Araujo et al., 2012; 2016). Foreland basin sediments of the Goiabeira schist of the Martinópole Group and Jaibaras Basin in the Borborema Province share similar detrital zircon age fractions to that of the Oti and Obosum groups and Kanti schist (Fig. 15c; Ganade de Araujo et al., 2012; 2016). The similarity in provenance pattern and depositional setting of the external zone of the Dahomeyide belt and sedimentary rocks of the Borborema Province provides important constraints on the assembly of West Gondwana during the Brasiliano/Pan-African orogeny and the reconstruction of pre-Gondwana paleogeography of West Africa and South America. A > 2500 km-long passive margin basin developed between ca. 1000 – 700 Ma before the onset of the assembly of West Gondwana, which was inverted during the Brasiliano/Pan-African plate convergence and collision, and the formation of the peripheral foreland basin.

8. Conclusions

Detailed field, petrographic, geochemical, and geochronological data have been used to constrain the provenance and depositional setting of the Buem structural unit sedimentary rocks. The Buem structural unit sedimentary rocks were deposited in a passive margin setting with sediments derived dominantly from the Amazonian Craton and minor contributions from the West African Craton. The geochemical and geochronological data reveal a strong correlation between the Buem structural unit, Togo structural unit and Voltaian Supergroup, an indication of similar depositional setting and provenance. Results from this study combined with previous data suggest two main sedimentary rocks in the external zone of the Dahomeyide belt, passive margin, and peripheral foreland basin which received detritus from probably the Amazonian Craton, Benino-Nigeran Shield, ± West African Craton. Geochronological data suggest the formation of a passive margin between 1000 and 700 Ma, followed by a foreland basin formation during subduction-collision at 750 – 570 Ma. Comparable data are available for the sedimentary rocks of the Borborema Province, NE Brazil, which imply similar evolution along the West Gondwana Orogen during the break-up of Rodinia and subsequent assembly of the supercontinent Gondwana. Because a greater portion of the detritus is from the Amazonian Craton, the coexistence of the West African and the Amazonian cratons from the Paleoproterozoic with no major oceans between them until the opening of the Atlantic Ocean is proposed.

CRediT authorship contribution statement

Daniel Kwayisi: Conceptualization, Methodology, Investigation, Writing – original draft. **Jeremie Lehmann:** Supervision, Writing – review & editing. **Marlina Elburg:** Supervision, Writing – review & editing.

Declaration of Competing Interest

The authors declare that they have no known competing financial interests or personal relationships that could have appeared to influence the work reported in this paper.

Acknowledgments

The authors acknowledge the financial support provided by the National Research Foundation (NRF) of South Africa, grant (105451), the African-German Network of Excellence in Science (AGNES) Mobility Grant 2018, Paleoproterozoic Mineralization (PPM) group of the University of Johannesburg, Department of Geology, DSI-NRF Centre of Excellence for Integrated Mineral and Energy Resource Analysis (CIMERA), and the College of Basic and Applied Sciences (CBAS), University of Ghana. Our heartfelt appreciation goes to Dr Jacob M. Kutu, the Nyavor family, Mr Emmanuel Nyavor, Mr Emmanuel Kwaku Awunyo, the Chief and people of Bontibor, Nkwanta, Chiaso, Nkonya-Mangoase, Aburuburuwa, Asukawkaw, Kanease, and Akyem for their support during the fieldwork. We are grateful to the Geological Survey Department of Ghana for the release of vehicle for the fieldwork. The authors would like to show appreciation to the Editor and two reviewers Udo Zimmermann and Daniel T. Brennan for taking their time to review the manuscript.

Appendix A. Supplementary material

Supplementary data to this article can be found online at https://doi.org/10.1016/j.gr.2022.04.020.

References

Abati, J., Aghzer, A.M., Gerdes, A., Ennih, N., 2012. Insights on the crustal evolution of the West African Craton from Hf isotopes in detrital zircons from the Anti-Atlas belt. Precambr. Res. 212-213, 263–274.

Abdelsalam, M.G., Liégeois, J.-P., Stern, R.J., 2002. The Saharan metacraton. J. Afr. Earth Sci. 34 (3-4), 119–136.
Abouchami, W., Boher, M., Michard, A., Albarede, F., 1990. A major 2.1 Ga event of mafic magmatism in West Africa: an early stage of crustal accretion. J. Geophys. Res. Solid Earth 95 (B11), 17605–17629.
Abu, M., Zango, M.S., 2017. Geochemical characteristics of the Neoproterozoic Anyaboni sandstone of the southeastern Voltaian Basin Ghana. *Scientific Res. J. (SCIRJ)* 5 (11), 54–65.
Adjei, A.O., Tetteh, G.M., 1997. Deformational phases of the Togo series, Ho-Nyive-Honuta area Ghana. *Ghana Mining J.* 3 (1), 1–9.
Affaton, P., 1990. Le bassin des Volta (Afrique de l'Ouest): une marge passive, d'âge protérozoïque supérieur, tectonisée au Panafricain (600 plus ou moins 50 Ma). In: Thèse Doctorat d'Etat, collections Etude et Thèse, p. 499.
Affaton, P., Kröner, A., Seddoh, K.F., 2000. Pan-African granulite formation in the Kabye Massif of northern Togo (West Africa): Pb− Pb zircon ages. Int. J. Earth Sci. 88 (4), 778–790.
Affaton, P., Aguirre, L., Ménot, R.P., 1997. Thermal and geodynamic setting of the Buem volcanic rocks near Tiéle, Northwest Benin West Africa. Precambr. Res. 82, 191–209.
Affaton, P., Rahaman, M.A., Trompette, R., Sougy, J., 1991. The Dahomeyide Orogen: tectonothermal evolution and relationships with the Volta Basin. In: Dallmeyer, R.D., Lécorché, J.P. (Eds.), The West African Orogens and Circum-Atlantic Correlatives. Springer Berlin Heidelberg, Berlin, Heidelberg, pp. 107–122. https://doi.org/10.1007/978-3-642-84153-8_6.
Affaton, P., Sougy, J., Trompette, R., 1980. The tectonostratigraphic relationships between the upper Precambrian and lower Paleozoic Volta Basin and the pan-African Dahomeyide orogenic belt (West Africa). Am. J. Sci. 280 (3), 224–248.
Agbossoumonde, Y., Menot, R.-P., Guillot, S., 2001. Metamorphic evolution of Neoproterozoic eclogites from south Togo (West Africa). J. Afr. Earth Sci 33 (2), 227–244.
Agyei, E.K., Van Landewijk, J.E.J.M., Armstrong, R.L., Harakal, J.E., Scott, K.L., 1987. Rb/Sr and K/Ar geochronometry of southeastern Ghana. J. Afr. Earth Sci. (1983), 6(2), 153–161.
Aidoo, F., Nude, P.M., Dampare, S.B., Agbossoumondè, Y., Salifu, M., Appenteng, M.K., Tulasi, D., 2014. Geochemical Characteristics of Granitoids (Ho Gneiss) from the Pan-African Dahomeyide Belt, Southeastern, Ghana: Implications for Petrogenesis and Tectonic Setting. J. Environ. Earth Sci. 4, 46–65.
Amedjoe, C.G., Gawu, S.K.Y., Ali, B., Aseidu, D.K., Nude, P.M., 2018. Geochemical compositions of Neoproterozoic to Lower Palaeozoic (?) shales and siltstones in the Volta Basin (Ghana): Constraints on provenance and tectonic setting. Sediment. Geol. 368, 114–131.
Anani, C., 1999. Sandstone petrology and provenance of the Neoproterozoic Voltaian Group in the southeastern Voltaian Basin Ghana. *Sediment. Geol.* 128 (1-2), 83–98.
Anani, C.Y., Bonsu, S., Kwayisi, D., Asiedu, D.K., 2019. Geochemistry and provenance of Neoproterozoic metasedimentary rocks from the Togo structural unit Southeastern Ghana. *J. Afr. Earth Sci.* 153, 208–218.
Anani, C.Y., Mahamuda, A., Kwayisi, D., Asiedu, D.K., 2017. Provenance of sandstones from the Neoproterozoic Bombouaka Group of the volta Basin, northeastern Ghana. Arabian J. Geosci. 10 (21), 465.
Anani, C., Moradeyo, M., Atta-Peters, D., Kutu, J., Asiedu, D., Boamah, D., 2013. Geochemistry and provenance of sandstones from Anyaboni and surrounding areas in the voltaian basin, Ghana. Int. Res. J. Geol. and Min. 6, 206–212.
Andersen, T., Kristoffersen, M., Elburg, M.A, 2016. How far can we trust provenance and crustal evolution information from detrital zircons? A South African case study. Gondwana Res. 34, 129–148.
Andersen, T., Kristoffersen, M., Elburg, M.A., 2018. Visualizing, interpreting and comparing detrital zircon age and Hf isotope data in basin analysis–a graphical approach. Basin Res. 30 (1), 132–147.
Anum, S., Sakyi, P.A., Su, B.-X., Nude, P.M., Nyame, F., Asiedu, D., Kwayisi, D., 2015. Geochemistry and geochronology of granitoids in the Kibi-Asamankese area of the Kibi-Winneba volcanic belt, southern Ghana. J. Afr. Earth Sci. 102, 166–179.
Antonio, P.Y., Baratoux, L., Trindade, R.I., Rousse, S., Ayite, A., Lana, C., Macouin, M., Adu, E.W., Sanchez, C., Silva, M.A., Firmin, A.S., 2021. West Africa in Rodinia: High quality paleomagnetic pole from the∼ 860 Ma Manso dyke swarm (Ghana). Gondwana Res., 28–43
Attoh, K., 1998. High-pressure granulite facies metamorphism in the Pan-African Dahomeyide orogen West Africa. *The J. Geol.* 106 (2), 236–246.
Attoh, K., Nude, P.M., 2008. Tectonic significance of carbonatite and ultrahigh-pressure rocks in the Pan-African Dahomeyide suture zone, southeastern Ghana. Geol. Soc. Lond., Spec. Publ. 297 (1), 217–231.
Attoh, K., Dallmeyer, R.D., Affaton, P., 1997. Chronology of nappe assembly in the Pan-African Dahomeyide orogen, West Africa: evidence from ^{40}Ar-^{39}Ar mineral ages. Precambrian Res. 82 (1–2), 153–171.
Attoh, K., Hawkings, G., Bowring, S.A., 1991. U-Pb zircon ages from the Pan-African Dahomeyide orogen, West Africa. EOS Trans. *Am. Geophys. Union Spring Meeting* 72, abstract.
Attoh, K., Corfu, F., Nude, P., 2007. U-Pb zircon age of deformed carbonatite and alkaline rocks in the Pan-African Dahomeyide suture zone West Africa. *Precambr. Res.* 155 (3-4), 251–260.
Attoh, K., Samson, S., Agbossoumondé, Y., Nude, P.M., Morgan, J., 2013. Geochemical characteristics and U-Pb zircon LA-ICPMS ages of granitoids from the Pan-African Dahomeyide orogen West Africa. *J. Afr. Earth Sci.* 79, 1–9.
Baratoux, L., Metelka, V., Naba, S., Jessell, M.W., Grégoire, M., Ganne, J., 2011. Juvenile Paleoproterozoic crust evolution during the Eburnean orogeny (∼ 2.2-2.0 Ga), western Burkina Faso. Precambr. Res. 191 (1-2), 18–45.
Baratoux, L., Söderlund, U., Ernst, R.E., De Roever, E., Jessell, M.W., Kamo, S., Naba, S., Perrouty, S., Metelka, V., Yatte, D., Grenholm, M., 2019. New U–PB baddeleyite ages of mafic dyke swarms of the West African and amazonian cratons: Implication for their configuration in supercontinents through time. In *Dyke Swarms of the World: A Modern Perspective,* Springer, Singapore, 263–314.
Barfod, G.H., Vervoort, J.D., Montanez, I.P., Riebold, S., 2004. Lu-Hf geochronology of phosphates in ancient sediments. 13th Goldschmith conference, Copenhagen, *Geochim. Cosmochim. Acta*, *abstract, 68*(11), A336.
Berger, J., Caby, R., Liégeois, J.-P., Mercier, J.-C., Demaiffe, D., 2011. Deep inside a neoproterozoic intra-oceanic arc: growth, differentiation and exhumation of the Amalaoulaou complex (Gourma, Mali). Contrib. Miner. Petrol. 162 (4), 773–796.
Black, R., 1967. Sur l'ordonnance des chaînes métamorphiques en Afrique occidentale. Chronicle of Mines Research, Min. Paris 364, 225–238.
Blay, P.K., 1983. The stratigraphic correlation of the Afram Shales of Ghana West Africa. *J. Afr. Earth Sci.* 1 (1), 9–16.
Block, S., Baratoux, L., Zeh, A., Laurent, O., Bruguier, O., Jessell, M., Ailleres, L., Sagna, R., Parra-Avila, L.A., Bosch, D., 2016. Paleoproterozoic juvenile crust formation and stabilisation in the south-eastern West African Craton (Ghana); New insights from U-Pb-Hf zircon data and geochemistry. Precambr. Res. 287, 1–30.
Boger, S., Raetz, M., Giles, D., Etchart, E., Fanning, C., 2005. U-Pb age data from the Sunsas region of Eastern Bolivia, evidence for the allochthonous origin of the Paragua Block. Precambr. Res. 139 (3-4), 121–146.
Bouvier, A., Vervoort, J.D., Patchett, P.J., 2008. The Lu-Hf and Sm-Nd isotopic composition of CHUR: constraints from unequilibrated chondrites and implications for the bulk composition of terrestrial planets. Earth Planet. Sci. Lett. 273 (1-2), 48–57.
Bozhko, N.A., 1969. Division et corrélation des dépôts du Précambrien supérieur de la plateforme africaine. Traduit de ''Vestnik Moskoskogo Universiteta. Geologiia i Rasviedka 5, 21–26.
Caby, R., 2003. Terrane assembly and geodynamic evolution of central-western Hoggar: a synthesis. J. Afr. Earth Sci. 37 (3-4), 133–159.
Caby, R., 2014. Nature and evolution of Neoproterozoic ocean-continent transition: Evidence from the passive margin of the West African craton in NE Mali. J. Afr. Earth Sci. 91, 1–11.
Carney, J.N., Jordan, C.J., Thomas, C.W., Condon, D.J., Kemp, S.J., Duodo, J.A., 2010. Lithostratigraphy, sedimentation and evolution of the Volta Basin in Ghana. Precambr. Res. 183 (4), 701–724.
Clauer, N., 1976. Isotopic geochemistry of strontium in sedimentary environments. Application to the geochronology of the cover of the West African craton. *Persée-Portal of scientific j*. SHS 45, (1).
Clauer, N., Caby, R., Jeannette, D., Trompette, R., 1982. Geochronology of sedimentary and metasedimentary Precambrian rocks of the West African craton. Precambr. Res. 18 (1-2), 53–71.
Condie, K.C., 1993. Chemical composition and evolution of the upper continental crust: contrasting results from surface samples and shales. Chem. Geol. 104 (1-4), 1–37.
Condie, K.C., Belousova, E., Griffin, W.L., Sircombe, K.N., 2009. Granitoid events in space and time: constraints from igneous and detrital zircon age spectra. Gondwana Res. 15 (3-4), 228–242.
Cordani, U.G., Teixeira, W., 2007. Proterozoic accretionary belts in the Amazonian Craton. Geol. Soc. Am. Mem. 200, 297–320.
Cordani, U.G., Pimentel, M.M., Ganade De Araujo, C.E., Basei, M.A.S., Fuck, R.A., Girardi, V.A.V., 2013. Was there an Ediacaran Clymene ocean in central South America? Am. J. Sci. 313 (6), 517–539.
Cordani, U.G., Teixeira, W., D'Agrella-Filho, M.S., Trindade, R.I., 2009. The position of the Amazonian Craton in supercontinents. Gondwana Res. 15 (3-4), 396–407.
Cordani, U.G., D'Agrella-Filho, M.S., Brito-Neves, B.B., Trindade, R.I.F., 2003. Tearing up Rodinia: the Neoproterozoic palaeogeography of South American cratonic fragments. Terra Nova 15 (5), 350–359.
Corfu, F., Hanchar, J.M., Hoskin, P.W., Kinny, P., 2003. Atlas of zircon textures. Rev. Miner. Geochem. 53 (1), 469–500.
Cullers, R.L., 1994. The controls on the major and trace element variation of shales, siltstones, and sandstones of Pennsylvanian-Permian age from uplifted continental blocks in Colorado to platform sediment in Kansas, USA. Geochim. Cosmochim. Acta 58 (22), 4955–4972.
Cullers, R.L., Podkovyrov, V.N., 2000. Geochemistry of the Mesoproterozoic Lakhanda shales in southeastern Yakutia, Russia: implications for mineralogical and provenance control, and recycling. Precambr. Res. 104 (1–2), 77–93.
Delor, C., de Roever, E.W.F., Lafon, J.M., 2003. The Bakhuis ultrahigh-temperature granulite belt (Suriname): Transamazonian crustal stretching in the revised Guiana Shield framework. Geol. Fr. 2, 207–230.
Deynoux, M., Affaton, P., Trompette, R., Villeneuve, M., 2006. Pan-African tectonic evolution and glacial events registered in Neoproterozoic to Cambrian cratonic and foreland basins of West Africa. J. Afr. Earth Sci. 46 (5), 397–426.
Dickinson, W.R., Beard, L.S., Brakenridge, G.R., Erjavec, J.L., Ferguson, R.C., Inman, K. F., Knepp, R.A., Lindberg, F.A., Ryberg, P.T., 1983. Provenance of North American Phanerozoic sandstones in relation to tectonic setting. Geol. Soc. Am. Bull. 94 (2), 222. https://doi.org/10.1130/0016-7606(1983)94<222:PONAPS>2.0.CO;210.1130/8302.
Duclaux, G., Ménot, R.P., Guillot, S., Agbossoumondé, Y., Hilairet, N., 2006. The mafic layered complex of the Kabyé massif (north Togo and north Bénin): Evidence of a Pan-African granulitic continental arc root. Precambr. res. 151 (1–2), 101–118.
Egal, E., Thiéblemont, D., Lahondère, D., Guerrot, C., Costea, C.A., Iliescu, D., Delor, C., Goujou, J.-C., Lafon, J.M., Tegyey, M., Diaby, S., Kolié, P., 2002. Late Eburnean

granitization and tectonics along the western and northwestern margin of the Archean Kénéma-Man domain (Guinea, West African Craton). Precambr. Res. 117 (1-2), 57–84.
Ennih N, Liégeois, J.P., 2008. The boundaries of the West African craton, with a special reference to the basement of the Moroccan metacratonic Anti-Atlas belt. In: Ennih N, Liégeois JP (eds) The boundaries of the West African craton, vol 297. *Geol. Soc. Lond. Spec Publ.* 1–17.
Evans, D.A.D., 2009. The palaeomagnetically viable, long-lived and all-inclusive Rodinia supercontinent reconstruction. Geol. Soc. Lond. Specl Publ. 327 (1), 371–404.
Evans, D.A.D., 2013. Reconstructing pre-Pangean supercontinents. *Bull.* 125 (11-12), 1735–1751.
Floyd, P.A., Leveridge, B.E., 1987. Tectonic environment of the Devonian Gramscatho basin, south Cornwall: framework mode and geochemical evidence from turbiditic sandstones. J. Geol. Soc. 144 (4), 531–542.
Ganade de Araujo, C.E., Cordani, U.G., Weinberg, R.F., Basei, M.A.S., Armstrong, R., Sato, K., 2014a. Tracing Neoproterozoic subduction in the Borborema Province (NE-Brazil): Clues from U-Pb geochronology and Sr-Nd-Hf-O isotopes on granitoids and migmatites. Lithos 202-203, 167–189.
Ganade de Araujo, C.E., Weinberg, R.F., Cordani, U.G., 2014b. Extruding the Borborema Province (NE Brazil): a two-stage Neoproterozoic collision process. Terra Nova 26 (2), 157–168.
Ganade de Araujo, C.E., Rubatto, D., Hermann, J., Cordani, U.G., Caby, R., Basei, M.A., 2014c. Ediacaran 2,500-km-long synchronous deep continental subduction in the West Gondwana Orogen. Nat. Commun. 5 (1), 1–8.
de Araujo, C.E.G., Cordani, U.G., Basei, M.A.S., Castro, N.A., Sato, K., Sproesser, W.M., 2012. U-Pb detrital zircon provenance of metasedimentary rocks from the Ceará Central and Médio Coreaú Domains, Borborema Province, NE-Brazil: tectonic implications for a long-lived Neoproterozoic active continental margin. Precambr. Res. 206-207, 36–51.
Ganade de Araujo, C.E., Cordani, U.G., Agbossoumounde, Y., Caby, R., Basei, M.A., Weinberg, R.F., Sato, K., 2016. Tightening-up NE Brazil and NW Africa connections: New U-Pb/Lu-Hf zircon data of a complete plate tectonic cycle in the Dahomey belt of the West Gondwana Orogen in Togo and Bénin. Precambr. Res. 276, 24–42.
Ghana National Geological Map Project, 2009. Geological Survey Department of Ghana and Bundesanstalt fur Geowiessenschaften und Rohstoffe (BGR), Germany.
Gray, D.R., Foster, D.A., Meert, J.G., Goscombe, B.D., Armstrong, R., Trouw, R.A.J., Passchier, C.W., 2008. A Damara orogen perspective on the assembly of southwestern Gondwana. Geol. Soc. Lond. Spec. Publ. 294 (1), 257–278.
Grant, N.K., 1969. The late Precambrian to early Paleozoic Pan-African orogeny in Ghana, Togo, Dahomey, and Nigeria. Geol. Soc. Am. Bull. 80 (1), 45–56.
Grenholm, M., Jessell, M., Thébaud, N., 2019. A geodynamic model for the Paleoproterozoic (ca. 2.27–1.96 Ga) Birimian Orogen of the southern West African Craton-Insights into an evolving accretionary-collisional orogenic system. Earth Sci. Rev. 192, 138–193.
Griffin, W.L., Belousova, E.A., Shee, S.R., Pearson, N.J., O'Reilly, S.Y., 2004. Archean crustal evolution in the northern Yilgarn Craton: U-Pb and Hf-isotope evidence from detrital zircons. Precambr. Res. 131 (3-4), 231–282.
Guillot, S., Agbossoumondé, Y., Bascou, J., Berger, J., Duclaux, G., Hilairet, N., Ménot, R.-P., Schwartz, S., 2019. Transition from subduction to collision recorded in the Pan-African arc complexes (Mali to Ghana). Precambr. Res. 320, 261–280.
Hirdes, W., Davis, D.W., 2002. U-Pb zircon and rutile metamorphic ages of Dahomeyan garnet-hornblende gneiss in southeastern Ghana West Africa. *J. Afr. Earth Sci.* 35 (3), 445–449.
Hoskin, P.W., Schaltegger, U., 2003. The composition of zircon and igneous and metamorphic petrogenesis. Rev. Miner. Geochem. 53 (1), 27–62.
Jessell, M., Santoul, J., Baratoux, L., Youbi, N., Ernst, R.E., Metelka, V., Miller, J., Perrouty, S., 2015. An updated map of West African mafic dykes. J. Afr. Earth Sci. 112, 440–450.
Jiang, Y.D., Schulmann, K., Kröner, A., Sun, M., Lexa, O., Janoušek, V., Buriánek, D., Yuan, C., Hanžl, P., 2017. Neoproterozoic-Early Paleozoic Peri-Pacific Accretionary Evolution of the Mongolian College System: Insights From Geochemical and U-Pb Zircon Data From the Ordovician Sedimentary Wedge in the Mongolian Altai. Tectonics 36 (11), 2305–2331.
Jordan, T.E., 1981. Thrust loads and foreland basin evolution, Cretaceous, western United States. AAPG bull 65 (12), 2506–2520.
Junner, N.R., Hirst, T., 1946. The geology and hydrogeology of Voltaian basin: Gold Coast Geological Survey Department. Memoir No. 8, Accra, 51.
Kah, L.C., Bartley, J.K., Teal, D.A., 2012. Chemostratigraphy of the Late Mesoproterozoic Atar Group, Taoudeni Basin, Mauritania: Muted isotopic variability, facies correlation, and global isotopic trends. Precambr. Res. 200-203, 82–103.
Kalsbeek, F., Affaton, P., Ekwueme, B., Frei, R., Thrane, K., 2012. Geochronology of granitoid and metasedimentary rocks from Togo and Bénin, West Africa: comparisons with NE Brazil. Precambr. Res. 196, 218–233.
Kalsbeek, F., Frei, R., 2010. Geochemistry of Precambrian sedimentary rocks used to solve stratigraphical problems: an example from the Neoproterozoic Volta basin Ghana. Precambr. Res. 176 (1-4), 65–76.
Kalsbeek, F., Frei, D., Affaton, P., 2008. Constraints on provenance, stratigraphic correlation and structural context of the Volta basin, Ghana, from detrital zircon geochronology: An Amazonian connection? Sediment. Geol. 212 (1-4), 86–95.
Kalsbeek, F., Frei, D., Schersten, A., Frei, R., Gerdes, A., Kalvig, P., 2020. Enigmatic 1146±4 Ma old granite in the southeastern rim of the West African craton, now part of the Dahomeyan orogenic belt in Ghana. J. Afr. Earth Sci. 103814.
Kinny, P.D., Wijbrans, J.R., Froude, D.O., Williams, I.S., Compston, W., 1990. Age constraints on the geological evolution of the Narryer Gneiss Complex Western Australia. Australian J. Earth Sci. 37 (1), 51–69.
Kouamelan, A.N., Delor, C., Peucat, J.J., 1997. Geochronological evidence for reworking of Archean terrains during the early Proterozoic (2.1 Ga) in the western Cote d'Ivoire (Man Rise-West African Craton). Precambr. Res. 86 (3–4), 177–199.
Kouamelan, A.N., Djro, S.C., Allialy, M.E., Paquette, J.-L., Peucat, J.-J., 2015. The oldest rock of Ivory Coast. J. Afr Earth Sci. 103, 65–70.
Kwayisi, D., Lehmann, J., Elburg, M., 2020. The architecture of the Buem Structural Unit: Implications for the tectonic evolution of the Pan-African Dahomeyide Orogen West Africa. Precambr. Res. 338, 105568. https://doi.org/10.1016/j.precamres.2019.105568.
Lafon, J.M., Delor, C., Guerrot, C., Lahondère, D., 2003. Archean crustal remnants in the easternmost part of the Guiana Shield: Pb-Pb and Sm-Nd geochronological evidence for Mesoarchean versus Neoarchean signatures. Geol. Fr. (2-3-4), 83–99
Ledru, P., Johan, V., Milési, J.P., Tegyey, M., 1994. Markers of the last stages of the Palaeoproterozoic collision: evidence for a 2 Ga continent involving circum-South Atlantic provinces. Precambr. Res. 69 (1-4), 169–191.
McLennan, S.M., 1989. Rare earth elements in sedimentary rocks: influence of provenance and sedimentary processes. Geochem. Mineral. Rare Earth Elements Rev. Miner. 21, 169–200.
McLennan, S.M., 1993. Weathering and global denudation. J. Geol. 101 (2), 295–303.
McLennan, S.M., Hemming, S., McDaniel, D.K., Hanson, G.N., 1993. Geochemical approaches to sedimentation, provenance, and tectonics. *Special Papers-Geol. Soc. Am.* 21–21.
Meert, J.G., 2012. What's in a name? The Columbia (Paleopangaea/Nuna) supercontinent. Gondwana Res. 21 (4), 987–993.
Nesbitt, H.W., Young, G.M., 1982. Early Proterozoic climates and plate motions inferred from major element chemistry of lutites. Nature 299 (5885), 715–717.
Milhomem Neto, J.M., Lafon, J.-M., 2019. Zircon U-Pb and Lu-Hf isotope constraints on Archean crustal evolution in Southeastern Guyana Shield. Geosci. Front. 10 (4), 1477–1506.
Nude, P.M., Kwayisi, D., Taki, N.A., Kutu, J.M., Anani, C.Y., Banoeng-Yakubo, B., Asiedu, D.K., 2015. Petrography and chemical evidence for multi-stage emplacement of western Buem volcanic rocks in the Dahomeyide orogenic belt, southeastern Ghana West Africa. *J. Afr. Earth Sci.* 112, 314–327.
Osae, S., Asiedu, D.K., Banoeng-Yakubo, B., Koeberl, C., Dampare, S.B., 2006. Provenance and tectonic setting of Late Proterozoic Buem sandstones of southeastern Ghana: Evidence from geochemistry and detrital modes. J. Afr. Earth Sci. 44 (1), 85–96.
Parra-Avila, L.A., Kemp, A.I.S., Fiorentini, M.L., Belousova, E., Baratoux, L., Block, S., Jessell, M., Bruguier, O., Begg, G.C., Miller, J., Davis, J., McCuaig, T.C., 2017. The geochronological evolution of the Paleoproterozoic Baoulé-Mossi domain of the southern West African Craton. Precambr. Res. 300, 1–27.
Pepper, M., Gehrels, G., Pullen, A., Ibanez-Mejia, M., Ward, K.M., Kapp, P., 2016. Magmatic history and crustal genesis of western South America: Constraints from U-Pb ages and Hf isotopes of detrital zircons in modern rivers. Geosphere 12 (5), 1532–1555.
Petersson, A., Scherstén, A., Gerdes, A., 2018. Extensive reworking of Archaean crust within the Birimian terrane in Ghana as revealed by combined zircon U-Pb and Lu-Hf isotopes. Geosci. Front. 9 (1), 173–189.
Potrel, A., Peucat, J.J., Fanning, C.M., 1998. Archean crustal evolution of the West African Craton: example of the Amsaga Area (Reguibat Rise). U-Pb and Sm-Nd evidence for crustal growth and recycling. Precambr. Res. 90 (3-4), 107–117.
Rogers, J.J.W., 1996. A history of continents in the past three billion years. The J. Geol. 104 (1), 91–107.
Rogers, J.J.W., Santosh, M., 2002. Configuration of Columbia, a Mesoproterozoic supercontinent. Gondwana Res. 5 (1), 5–22.
Rollinson, H., 2016. Archaean crustal evolution in West Africa: A new synthesis of the Archaean geology in Sierra Leone, Liberia Guinea and Ivory Coast. Precambr. Res. 281, 1–12.
Rooney, A.D., Selby, D., Houzay, J.-P., Renne, P.R., 2010. Re-Os geochronology of a Mesoproterozoic sedimentary succession, Taoudeni basin, Mauritania: Implications for basin-wide correlations and Re-Os organic-rich sediments systematics. Earth Planet. Sci. Lett. 289 (3-4), 486–496.
da Rosa-Costa, L.T., Lafon, J.M., Delor, C., 2006. Zircon geochronology and Sm-Nd isotopic study: further constraints for the Archean and Paleoproterozoic geodynamical evolution of the southeastern Guiana Shield, north of Amazonian Craton Brazil. Gondwana Res. 10 (3-4), 277–300.
Rudnick, R.L., Gao, S., 2003. Composition of the continental crust. The crust 3, 1–64.
Sadowski, G.R., Bettencourt, J.S., 1996. Mesoproterozoic tectonic correlations between eastern Laurentia and the western border of the Amazon Craton. Precambr. Res. 76 (3-4), 213–227.
Sakyi, P.A., Su, B.-X., Anum, S., Kwayisi, D., Dampare, S.B., Anani, C.Y., Nude, P.M., 2014. New zircon U-Pb ages for erratic emplacement of 2213–2130 Ma Paleoproterozoic calc-alkaline I-type granitoid rocks in the Lawra Volcanic Belt of Northwestern Ghana West Africa. Precambr. Res. 254, 149–168.
Santos, J.O.S., Hartmann, L.A., Gaudette, H.E., Groves, D.I., Mcnaughton, N.J., Fletcher, I.R., 2000. A new understanding of the provinces of the Amazon Craton based on integration of field mapping and U-Pb and Sm-Nd geochronology. Gondwana Res. 3 (4), 453–488.
Santos, J.O.S., Potter, P.E., Reis, N.J., Hartmann, L.A., Fletcher, I.R., McNaughton, N.J., 2003. Age, source, and regional stratigraphy of the Roraima Supergroup and Roraima-like outliers in northern South America based on U-Pb geochronology. Geol. Soc. Am. Bull. 115 (3), 331–348.

Santos, J.O.S., Rizzotto, G.J., Potter, P.E., McNaughton, N.J., Matos, R.S., Hartmann, L. A., Chemale, F., Quadros, M.E.S., 2008. Age and autochthonous evolution of the Sunsás Orogen in West Amazon Craton based on mapping and U-Pb geochronology. Precambr. Res. 165 (3-4), 120–152.
Saunders, R.S., 1970. Early Palaeozoic Orogeny in Ghana. Foreland Stratigraphy and Structure. Geol. Soc. Am Bull. 81 (1), 233–240.
Söderlund, U., Patchett, P.J., Vervoort, J.D., Isachsen, C.E., 2004. The 176Lu decay constant determined by Lu-Hf and U-Pb isotope systematics of Precambrian mafic intrusions. Earth Planet. Sci. Lett. 219 (3-4), 311–324.
Straathof, G.B., 2011. Neoproterozoic low latitude glaciations: An African perspective.
Tassinari, C.C., Munhá, J.M., Teixeira, W., Palácios, T., Nutman, A.P., Sosa, C., Santos, A.P., Calado, B.O., 2004. The Imataca Complex, NW Amazonian Craton, Venezuela: crustal evolution and integration of geochronological and petrological cooling histories. *Episodes-Newsmagazine of the IUGS*, *27*(1), 3-12.
Tassinari, C.C.G., Teixeira, W., Nutman, A.P., Szabó, G.A., Mondin, M., Sato, K., 2001. Archean crustal evolution of the Imataca Complex, Amazonian Craton: Sm–Nd, Rb–Sr e U-Pb (SHRIMP) evidences. Simpósio de Geologia da Amazônia 7.
Tassinari, C.C.G., Bettencourt, J.S., Geraldes, M.C., Macambira, M.J.B., Lafon, J.M., 2000. The Amazon craton. In: Cordani, U.G., Milani, E.J., Thomaz-Filho, A., Campos, D.A. (Eds.), Tectonic evolution of South America: Rio de Janeiro, Brazil, 31st Inter. Geol, Con., pp. 41–95.
Taylor, P.N., Moorbath, S., Leube, A., Hirdes, W., 1992. Early Proterozoic crustal evolution in the Birimian of Ghana: constraints from geochronology and isotope geochemistry. Precambr. Res. 56 (1-2), 97–111.
Taylor, S.R., McLennan, S.M., 1985. The continental crust: its composition and evolution. Blackwell Scientific Publ, Oxford.
Tohver, E., D'Agrella-Filho, M.S., Trindade, R.I.F., 2006. Paleomagnetic record of Africa and South America for the 1200–500 Ma interval, and evaluation of Rodinia and Gondwana assemblies. Precambr. Res. 147 (3-4), 193–222.
Trompette, R., 1994. Geology of western Gondwana (2000–500 Ma): Pan-Africa-Brasiliano aggregation of South America and Africa. TRO. 55, 215–313.
Trompette, R., 2000. Gondwana evolution; its assembly at around 600 Ma. Comptes Rendus de l'Académie des Sciences-Series IIA-Earth Planet Sci. 330 (5), 305–315.
Tshibubudze, A., Hein, K.A.A., Peters, L.F.H., Woolfe, A.J., McCUAIG, T.C., 2013. Oldest U-Pb crystallisation age for the West African Craton From the Oudalan-Gorouol Belt of Burkina Faso. South Afr. J. Geol. 116 (1), 169–181.
Villeneuve, M., Cornée, J.J., 1994. Structure, evolution and palaeogeography of the West African craton and bordering belts during the Neoproterozoic. Precambr. Res. 69 (1-4), 307–326.
Whitney, D.L., Evans, B.W., 2010. Abbreviations for names of rock-forming minerals. Am. mineral. 95 (1), 185–187.